UNIVERSITY OF TWENTE.

Faculty of Engineering Technology

A Linearized Parameter Study Of A Friction Isolator System: Towards A Frequency Domain Design Guideline

Jasper A. Fix

MSc. Thesis Mechanical Engineering
August 2023

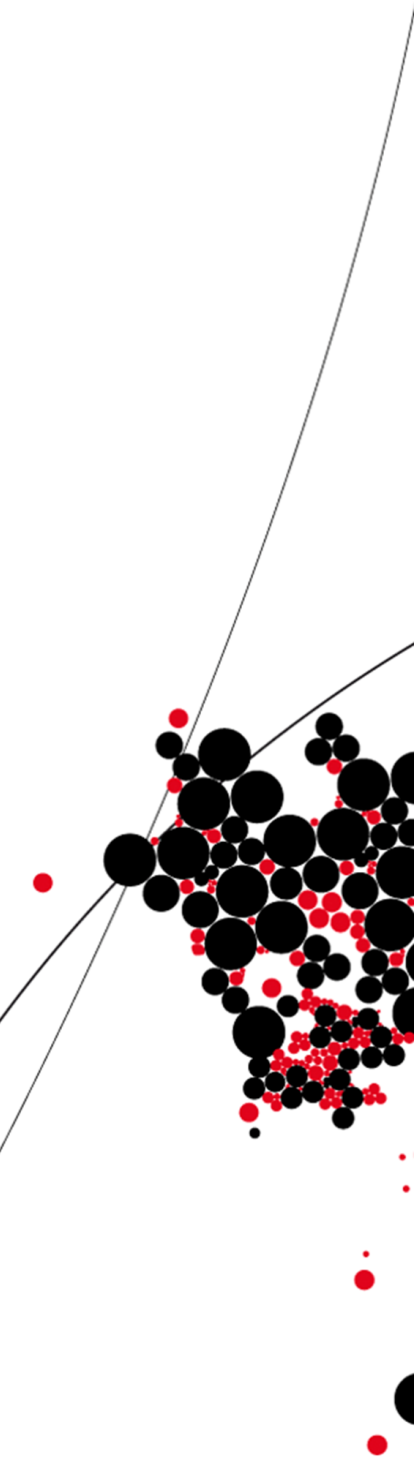

Supervisors:
Dr.ir. Jan J. de Jong EngD
Prof.dr.ir. Dannis M. Brouwer EngD

Chair of Precision Engineering
Faculty of Engineering Technology
University of Twente
P.O. Box 217
7500 AE Enschede
The Netherlands

Contents

1 Abstract

Nonlinear friction effects in linear guides can limit the positioning performance in high-precision systems. Stick-slip is one of these effects, through which a bearing makes a sudden transition from standstill to movement due to a nonlinear drop in friction force. Stick-slip in combination with an integral action in a typical PID controller can lead to hunting or friction induced limit cycles, which negatively affect the positioning performance of a servo system. In this study, a friction isolator that mitigates hunting through the addition of a compliant joint between the linear guide and the actuator is analyzed, designed, and tested. By combining the low linear stiffness of the compliant joint in series with the higher nonlinear pre-motion friction stiffness of the linear guide, the friction forces are linearized. Through simulations of a friction isolator with a LuGre friction model, the main system parameters are identified and design guidelines for a friction isolator are determined. From the parameter study, it was found that a friction isolator can be helpful in a system with limited control bandwidth and a significant gap between static and dynamic friction. Regarding the design of the friction isolator, it was found that the drive stiffness of the compliant joint should be as low as possible whilst the parasitic frequencies of the joint should be large enough not to limit the desired controller bandwidth. The stroke of the joint can be significantly smaller than the amplitude of the hunting cycles. The test setup build for this research, with an equivalent moving mass of 2.5 kg and static friction forces in the range from 1 to 2.5 N, saw hunting mitigation through the friction isolator with a control bandwidth of 5 Hz or larger. Which is significantly lower compared to the non-isolated system, which required a 15 Hz bandwidth. A stroke of 0.3 mm for the compliant joint is found to be sufficiently large for a satisfying performance of the friction isolator in this case. The experiments performed on the test setup agreed with the results of the parameter study.

2 Introduction

Contact-based bearings are widely used in positioning mechanisms for their relatively low cost and high support stiffness. However, in precise positioning, nonlinear friction forces in the bearings start to play a role and negatively affect the precision of the system [1]. Nonlinear friction phenomena can severely deteriorate the performance of controlled motion systems and lead to large tracking errors, unwanted oscillations, or hunting behavior [2, 3]. This hunting behavior, also called friction induced limit cycles, is a result of the combination of a controller with an integral action and a system containing a nonlinear transition between the static friction and smaller dynamic friction, the stick-slip effect [4, 5]. Hunting is a continuous and periodical positioning error, in which the system keeps oscillating around the desired position.

To prevent hunting from occurring in a positioning system, the integral action could be removed from the controller. Since this action reduces the steady state position error of a servo system, removing it could however be undesirable. Reduction of mechanical friction is another option to mitigate hunting cycles. Aerostatic bearings can be used to get rid of friction, but this type of bearing is often not suitable in clean-room environments and significantly increases the cost of a positioning system over using mechanical bearings [6].

An alternative method to decrease the friction in mechanical bearings is researched by Dong *et al.* [6], in which high frequency vibrations are exerted on the bearing rail in order to linearize the undesirable nonlinear friction effects like stick-slip. This method called vibration assisted nano-positioning (VAN), shows a decrease in settling time up to 52% without a significant increase in heat and wear in the system. Introducing vibration into a high-precision positioning system, however, might be unwanted due to parasitic vibrations in the end-effector that might decrease performance. To facilitate this, compliant joints are fitted between the bearings and

the end-effector, and a harmonic canceling controller is proposed to compensate for the parasitic vibrations. Nevertheless, using the VAN method increases the complexity and therewith the cost of a positioning system.

Later research by Dong *et al.* introduces the Compliant Joint Method or Friction Isolator (FI) [7–10], in which a compliant joint is used to connect the bearing and the end-effector of the system. This mechanical dual stage is proposed to compensate for nonlinear friction effects by placing a compliant linear spring in series with the higher and nonlinear pre-motion friction stiffness. This results in a system with a linearized friction force, which is more suitable to be controlled. Experimental results show mitigation of hunting cycles and improved settling times [8]. A schematic representation of the friction isolator system can be seen in Figure 1.

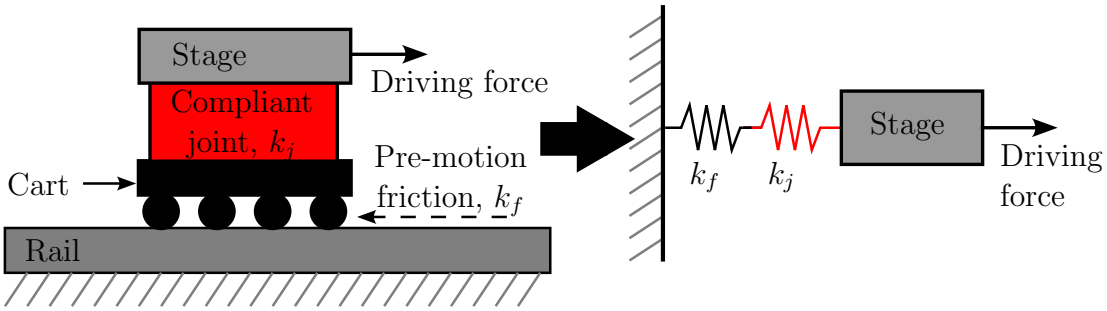

Figure 1: Schematic representation of the friction isolator system, in which the 'Stage' is to be positioned. Using a compliant joint with stiffness k_j, the stage is connected to the bearing, which is affected by pre-motion friction, with stiffness k_f.

Further improvements on the friction isolator system can be achieved by the use of more complex control methods, like active disturbance rejection control [11–15]. Some design aspects of the friction isolator have been researched for the case of applying active disturbance rejection control [12, 14] and stiffness and damping have been studied for evaluating the settling time and in-position stability [9]. However, many more parameters are of influence on the workings of a friction isolator, such as the system mass, traveled path, and control parameters. The influence of these parameters on the hunting behavior and the workings of a friction isolator is not always clear and a general guideline on designing a friction isolator is still missing.

In this research, a general design strategy will be presented for a friction isolator system. This strategy is based on a parameter study in combination with simulations, from which it is identified which system parameters influence the hunting behavior. A practical metric to identify hunting cycles from simulations was missing in literature and is therefore set up in this research as well. Further, a test setup is designed and built to experimentally verify the simulations and design method.

In Section 3 of this paper, the principle of the friction isolator will be discussed in more detail and the design parameters will be identified, after which the simulation setup will be discussed. This section will be concluded with the proposed design method for such a system and a description of the test setup. In Section 4, the results of the simulations will be discussed after which the test setup will be identified and the results of the experiments with the setup will be analyzed. This section is finished with a verification of the design method. Section 5 and 6 contain the discussion and the conclusion of this research respectively.

3 Method

3.1 The friction isolator

In the introduction, the idea of a friction isolator is briefly introduced. This section will elaborate on the working principles of the isolator. First, the stiffnesses playing a role in the friction isolator are discussed, after which the general design of such a system is illustrated and the analytical model is discussed.

3.1.1 Working principle

The basic system of a friction isolator consists of 2 masses, which are connected through a compliant joint. The compliance is facilitated by leafsprings. A schematic drawing of this type of system can be seen in Figure 2. The first mass of the system is the mass of the cart that rides on the bearing rail and is affected by the non-linear friction forces. The second mass is the mass of the compliant joint stage, which also is the end-effector. The actuator and position sensor are both connected to this mass.

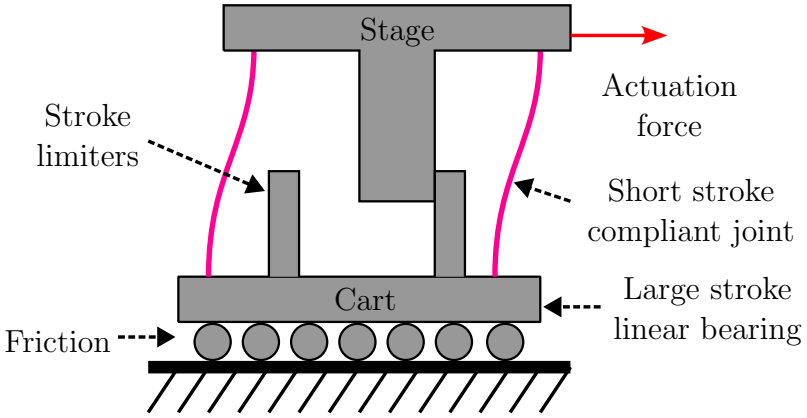

Figure 2: A schematic representation of a friction isolator. The actuation force positions the 'Stage', which is connected through the compliant joint with the bearing cart. Stroke limiters are used to limit the maximum stroke of the compliant joint.

The compliant joint, with stiffness k_j, works in series with the pre-motion friction of the bearing, which can be modeled as a spring with stiffness k_f. The stiffness of the pre-motion friction is very large at a standstill and drops rapidly to zero as the bearing starts moving, resulting in a highly nonlinear time- and position-varying friction force. The series connection of the stiffnesses can be seen in Figure 1. Note, the mass of the cart is neglected in this figure, as to highlight the combination of the springs. By placing the compliant joint in series with this pre-motion friction, the stiffness of the joint can be made dominant, thus working around the non-linear stiffness in the pre-motion regime. The combined effective stiffness, k_e, can be calculated as follows [7–9]:

$$k_e = \frac{k_f k_j}{k_f + k_j} \tag{1}$$

From this equation, it follows that the stiffness of the compliant joint is dominant over the pre-motion friction when the stiffness of the joint is significantly lower, thus $k_j \ll k_f$. The sensitivity of k_e to k_f is determined by:

$$\frac{\delta k_e}{\delta k_f} = \left(\frac{\eta}{1+\eta}\right)^2, \; with \; \eta = \frac{k_j}{k_f} \tag{2}$$

So, if $k_j \ll k_f$, $\eta \to 0$ the sensitivity of k_e to errors in k_f becomes very small. Thus, the system is more predictable since k_j is a more compliant and linear spring compared to the stiff non-linear k_f [7], resulting in a linearized friction force. This is easier to control for a feedback controller [8].

The stroke of the compliant joint, S_j, is defined as the distance from the neutral position of the joint to the stroke limiter on one side, the joint thus has a total deflection range of 2 times the stroke. Stroke limiters are used to prevent the compliant joint from high stresses and parasitic motion due to large deformations. The stroke limiters will be fitted in such a way that the force applied to the compliant joint is passed on to the cart through the stroke limiters when the end of the stroke is reached. It is expected that the size of the stroke has a minimum value for the friction isolator to be effective.

From the basic working principle of the friction isolator, the design parameters can be identified. These are the stiffness and damping of the compliant joint k_j and d_j, the stroke length of the joint S_j, the mass of the moving stage, including the actuator and sensor M_{stage}, and the stiffness and damping of the stroke limiters, k_l and d_l.

3.1.2 Analytical model

In this research, comparisons will be made between two systems, one with and one without the friction isolator. For both systems, an ideal physical model (IPM) is set up, which is used in the simulation model. The IPM of the system with the friction isolator is shown in Figure 3. The masses of the bearing cart and the positioning stage are modeled with their connecting components. A third mass is present in this model, which is used to model the first parasitic eigenfrequency of the system.

From the IPM, it can be seen that the springs and dampers connecting the fixed world to the cart and the cart to the flexure mechanism are variable, which means the system can be linearized into four limit cases: In the first case, only the flexure mechanism is moving and the bearing is being held in place by the static friction forces. The second case corresponds to the flexure mechanism and the bearing both moving independently. The third and fourth cases are similar, however, in these cases, the flexure mechanism is pushing the stroke limiters and thus experiences higher stiffness. The latter cases can be present when the force required to deflect the flexure mechanism to the end of the stroke is smaller than the static friction value in the bearing or during large acceleration or deceleration. An overview of the values for the stiffness and damping for the different cases can be found in Table 1.

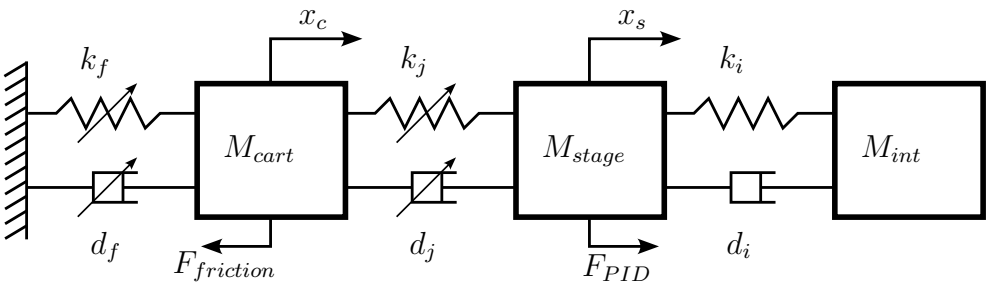

Figure 3: Ideal Physical Model (IPM) of a friction isolator. The mass of the cart is connected to the fixed world through k_f and d_f, which represent the friction in the bearing (M_{cart}). The values of the spring and damper depend on the velocity of the cart, either sticking or slipping of the bearing. k_j and d_j represent the stiffness and damping of the compliant joint that connect the positioning stage to the bearing cart. These values depend on the deflection of the joint, either values of the joint or the stroke limiters. The last mass represents the first parasitic frequency of the compliant joint. The controller force is applied to the stage mass.

Table 1: Parameter values of different linearized limit cases of the system.

Case	Cart velocity, v_c	Joint stroke, S_j	Frictional stiffness, k_f	Joint stiffness, k_j	Frictional damping, d_f	Joint damping, d_j
Case 1	0	$< S_{j,max}$	$k_{f,stick}$	k_j	$d_{f,stick}$	d_j
Case 2	$> v_s$	$< S_{j,max}$	$k_{f,slip}$	k_j	$d_{f,slip}$	d_j
Case 3	0	$S_{j,max}$	$k_{f,stick}$	$\frac{k_j k_l}{k_j+k_l}$	$d_{f,stick}$	$\frac{d_j d_l}{d_j+d_l}$
Case 4	$> v_s$	$S_{j,max}$	$k_{f,slip}$	$\frac{k_j k_l}{k_j+k_l}$	$d_{f,slip}$	$\frac{d_j d_l}{d_j+d_l}$

The system without the friction isolator will have the same mass and friction values as the system with the friction isolator. The IPM of the non-isolated system will reduce to the model shown in Figure 4, in which only one equivalent mass is present. This mass is equal to the combined mass of the cart and the positioning stage.

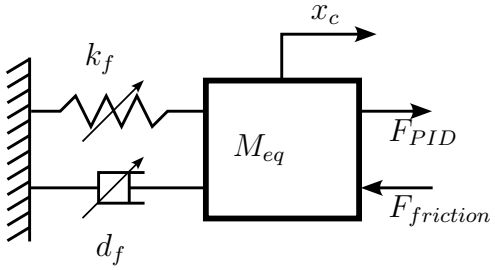

Figure 4: Ideal Physical Model (IPM) of the non-isolated case. The equivalent mass, $M_{eq} = M_{cart} + M_{stage}$, is connected to the fixed world through k_f and d_f, which represent the friction in the bearing. The values of the spring and damper depend on the velocity of the cart, either sticking or slipping of the bearing. The controller force is applied directly to the cart in this case.

3.2 Simulation setup

The goal of the simulations is to simulate the hunting behavior in the test setup that is to be designed and verify that the friction isolator mitigates this effect. To identify the most influential parameters for hunting and how these parameters affect hunting behavior, the IPM

is implemented in a Simulink model in combination with a LuGre friction model and a PID controller. Two models are made, one for the non-isolated system and one for the system with the friction isolator. The results of these simulations will be the outline for the design method of the friction isolator.

In this section, the LuGre friction model will be described, after which a metric to identify hunting cycles from a simulation is introduced. This is followed by a description of the simulation model and an introduction to the controller.

3.2.1 LuGre friction model

In a positioning system, the motion is often of point-to-point nature in which small displacements around accurate settling are alternated by large displacements between two settling points. For these different types of movements, two friction regimes can be identified: the pre-motion or pre-sliding regime and the rolling or gross sliding regime. In the rolling regime, the friction force is mainly dependent on the sliding velocity, whilst in the pre-sliding regime the friction is more affected by the elastoplastic deformations and micro-slip of the rolling elements. The transition between these friction regimes is highly nonlinear and can be abrupt, leading to stick-slip behavior in which an object is suddenly transitioned from standstill - 'stick' to movement - 'slip'. [1, 2].

The effects of friction in controlled systems have been extensively studied in literature, in order to model the friction force [3, 16]. A variety of friction models is available, ranging from simple general models to more complex and accurate models, containing different friction effects. One of the more complex models is the LuGre friction model [17, 18], which is accurate in modeling presliding friction and stick-slip effects [19].

In the LuGre model, the contact between two bodies at asperities is modeled as contact through elastic bristles. These bristles will deflect like springs when a tangential force is applied, leading to a friction force [17]. If the tangential force is large enough, bristles will start to slip. The friction behavior is based on the average bristle deflection, z, which is described by:

$$\frac{dz}{dt} = v - \sigma_0 \frac{|v|}{g(v)} z \tag{3}$$

In this equation, v is the relative velocity between the two bodies and $g(v)$ describes the Coulomb friction and the Stribeck effect, as:

$$g(v) = F_c + (F_s - F_c) e^{-(|\frac{v}{v_s}|)^j} \tag{4}$$

Where F_c is the Coulomb friction force, F_s is the stiction force and v_s is the Stribeck velocity. The parameter $j = 2$ [17].

The total friction force is described by:

$$F = \sigma_0 z + \sigma_1 \dot{z} + \sigma_2 v \tag{5}$$

The coefficients σ_0 and σ_1 describe the bristle stiffness and damping respectively. σ_2 is a parameter for the viscous damping of the model. The values for these parameters in this study are taken from literature [17].

All values for the parameters of the LuGre model are fixed and can be found in Table 2.

Table 2: Parameters of the LuGre model used in the simulations [17].

Symbol	Value	Unit	Description
σ_0	10^5	[N/m]	Bristle stiffness
σ_1	$\sqrt{10^5}$	[Ns/m]	Bristle damping
σ_2	0.5	[Ns/m]	Viscous damping
V_s	$1.6 \cdot 10^{-3}$	[m/s]	Stribeck velocity
F_s	3	[N]	Static friction force
F_c	1	[N]	Coulomb friction force

3.2.2 Quantification of hunting

Hunting cycles are a friction-induced phenomenon that occurs in the time domain. In order to identify whether the system is actually showing hunting in the simulation runs, a metric is required that describes the hunting characteristics. A practical metric to identify hunting cycles from a simulation result is not present in literature, therefore one is constructed here. From previous research [4, 20], it can be seen that the hunting cycles have a duration in the order of seconds, with an amplitude in the order of millimeters. A typical example of the position signal of a system affected by hunting can be seen in Figure 5.

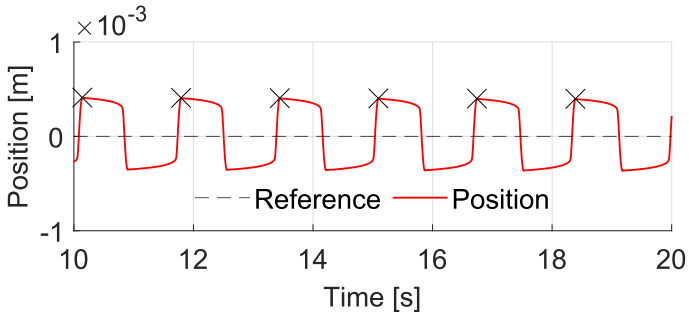

Figure 5: Position signal for a simulated system that is affected by hunting cycles. The markers indicate the identified peaks, that correspond to a hunting cycle.

In order to quantify the hunting behavior a simulation of 20 seconds is performed, in which the system is moved from a standstill at position 0 by means of two trapezoidal steps, in both directions. The acceleration value and time of acceleration are fixed for these steps and both steps are equal in size. The second step thus takes the system back to the start position, which happens at 5 seconds. The traveled path affects the hunting behavior since the friction in a real setup is time and position dependent. Therefore the travelled path is kept equal in all simulations in this research, unless otherwise noted.

To find out whether a system shows stable hunting cycles, ie. the system is continuously affected by hunting cycles, the number of peaks in the position signal is counted after 10 seconds. This provides sufficient time for the system to settle and if hunting cycles are observed, it can be stated that the system is affected by stable hunting cycles. The peaks are identified with a minimum time between the peaks of 0.5 seconds and a minimum peak height of 0.1 mm. Each hunting cycle will correspond to one peak. The markers in Figure 5 are an example of the identified peaks in the hunting cycles.

It should be noted however that the absolute amount of hunting cycles is not of importance, since a system could respond faster under certain parameters like mass or control parameters and thus show more hunting cycles than a slower system. If both show stable hunting cycles

though, both systems are impractical for use. Therefore it is more important whether peaks are identified after the system had some time to settle than the exact amount.

3.2.3 Model for simulations

The simulation models are based on the Ideal Physical Model (IPM) as shown in Figure 3 and 4. In the model of the non-isolated system, the stiffness and damping of the compliant joint are replaced by the stiffness and damping values of the stroke limiters. This is done since the masses of the cart and the positioning stage are always coupled through the contact stiffness of the stroke limiters of $k_l = 2 \cdot 10^7$ N/m. This type of connection is deemed more realistic than a rigid connection between both masses. The model that does contain the friction isolator does not have a constant value for the stiffness and damping of the compliant joint. It has either the value of the drive stiffness of the flexure mechanism or the value of the contact stiffness of the stroke limiters in the case that the maximum stroke of the mechanism is exceeded. For both models, the stiffness and damping coefficients of the spring and damper connecting the cart to the fixed world are variable according to the LuGre friction model.

Solver and solver tolerance

In Simulink, multiple types of solvers are available to solve the differential equations in the model. Often, the ODE45 solver based on the Dormand-Price algorithm is used. This solver often yields satisfactory results for non-stiff ODEs and is recommended by Matlab as the go-to solver. However, more accurate and more efficient algorithms are present. When stiff differential equations are to be solved, the ODE45 solver might become problematic and yield unstable results [21]. Such stiff differential equations are present in the LuGre friction model [18] and thus another solver type is required. Simulink has four stiff ODE solvers, of which ODE15s is the standard solver to use when a stiff problem is expected. In the simulations described in this section, ODE23s is used as the solver since this type is more efficient than the ODE15s solver and still yields accurate results.

Another important parameter in the simulations is the tolerance of the solver, which can affect the outcome significantly. The trade-off in the tolerance is the computation time such that a too strict tolerance is not wanted. The relative tolerance is set to 10^{-4}, as is the maximum step size [20].

3.2.4 Controller

The friction isolator will be controlled by a PID controller. This type of controller consists of three parts, as can be seen in the control law in Equation 6. K_p is the proportional gain which acts linearly on the error and ensures a faster response and smaller stationary error. The differential action, K_d adds damping to the controller to prevent oscillating behavior and enhance stability. This differential term also contains a parameter τ, which is a time constant that limits the high frequency gain of the controller. The last part is the integral action K_i, which integrates the error over time, thus making the system able to reduce stationary errors and making this type of controller suitable for positioning systems. Further, this type of controller is widely used in industry and is thus a representable option.

$$K(s) = K_p + \frac{K_i}{s} + \frac{K_d s}{s\tau + 1} \tag{6}$$

Tuning the controller is done by using the tuning rules of Van Dijk [22], in which all the gains are dependent on the desired cross-over frequency of the controller. The control law of Equation

6 can be rewritten in terms of the tunable parameters by Van Dijk:

$$K(s) = \frac{1}{\tau_p s + 1} \cdot k_p \left[\left(1 + \frac{\tau_z}{\tau_i} \right) + \frac{1}{\tau_i} \cdot \frac{1}{s} + \tau_z \cdot s \right] \tag{7}$$

$$\begin{aligned} \tau_z &= \frac{\sqrt{\frac{1}{\alpha}}}{\omega_c} \quad , \tau_i = \beta \cdot \tau_z \\ \tau_p &= \frac{1}{\omega_c \cdot \sqrt{\frac{1}{\alpha}}}, k_p = \frac{m_{eq} \omega_c^2}{\sqrt{\frac{1}{\alpha}}} \end{aligned} \tag{8}$$

This cross-over frequency determines the bandwidth of the system and with that the response time of the controller. The parameter α is a measure for the maximum phase lead and can thus affect the stability of the controlled system. The value is smaller than 1 and often chosen between 0.1 and 0.3. β affects the integral gain, in which it should be noted that $\tau_i \geq \tau_z$, thus $\beta \geq 1$.

3.3 Parameter study

A parameter study is conducted to find optimal parameters for the friction isolator and to study the effect of multiple parameters on the hunting behavior. The simulation model from Section 3.2 will be used to vary the parameters and analyze the resulting behavior. The study will be performed by creating multiple 2-d parameter grids to identify relations between these parameters and study the resulting behavior.

A distinction will be made in this study between the isolated and non-isolated system. The study on the non-isolated case will give insight into when hunting will occur and which parameters can be tuned in a linear guide positioning system in order to prevent hunting. For this case, the parameters that will be studied are the control parameters: ω_c, α and β and the system parameter mass: M_{eq}. Further, the static and coulomb friction will be taken into account, as well as the path the system travels. In the parameter grids, the parameters that are related are combined.

For the system with the friction isolator, the main parameters are the stroke of the compliant joint S_j, the drive stiffness k_j, damping of the stroke limiters d_l, and the cross-over frequency ω_c. The mass and friction parameters will be addressed in this case as well.

An overview of the studies that are performed with their corresponding parameter grids can be found in Table 3. The study names in this table will be used as a reference in the remainder of this research.

Table 3: Overview of the combined parameters in the parameter study.

Study name	Parameters	Symbol	Range
Path	Acceleration	a_{cart}	0 - 150 [m/s^2]
	Acceleration time	t_{acc}	0 - 0.15 [s]
System parameters	Cross-over frequency 1	$\omega_{c,1}$	1 - 40 [Hz]
	Mass	M_{eq}	0.1 - 5.1 [kg]
Friction forces	Static friction	F_s	0 - 4.9 [N]
	Coulomb friction	F_c	0 - 4.9 [N]
Control parameters	Alpha	α	0.1 - 0.3 [-]
	Beta	β	1 - 3 [-]
Friction isolator stiffness	Joint stiffness	k_j	$0.5{\cdot}10^3$ - $15{\cdot}10^3$ [N/m]
	Joint stroke 1	$S_{j,1}$	0 - $1 \cdot 10^{-3}$ [m]
Friction isolator damping	Damping coefficient	d_l	$10^{-2} - 10^4$ [Ns/m]
	Joint stroke 2	$S_{j,2}$	$10^{-5} - 10^{-2}$ [m]
Friction isolator cross-over	Cross-over 2	$\omega_{c,2}$	1 - 16 [Hz]
	Joint stroke 1	$S_{j,1}$	0 - $1 \cdot 10^{-3}$ [m]
Friction isolator mass	Bearing cart mass	M_{cart}	0.5 - 3 [kg]
	Positioning stage mass	M_{stage}	0.1 - 1 [kg]
Friction isolator friction forces	Static friction	F_s	0 - 4.9 [N]
	Coulomb friction	F_c	0 - 4.9 [N]

It is expected that the cross-over frequency of the controller will have the biggest influence on the behavior of the system, since this parameter determines the response time of the controller. With a faster response, the nonlinear changes in friction force can be accounted for faster, thus preventing large overshoot at breakaway of the bearing. This will affect both the isolated and non-isolated case. Next to that, the gap between the static and Coulomb friction force will affect the occurrence of hunting cycles, since this determines the stiction properties of the bearing. A larger gap is expected to lead to the occurrence of hunting cycles. Previous research showed some influence of the length and acceleration in the traveled path on the hunting behavior [8, 20], though no clear patterns are found.

In the isolated system, the allowed stroke of the compliant joint and the stiffness are expected to have the largest influence. A lower stiffness will be beneficial for the working principle of the isolator according to Section 3.1.1. A limit is expected to be found, above which the joint stiffness will be too large for the friction isolator to be effective. Since the amplitude of the hunting cycles is in the order of millimeters, the stroke is expected to be in the same order of magnitude, such that the compliant joint can facilitate the stage to reach the final position while the bearing sticks due to friction.

Experiments will be performed to verify the simulations. Identifications of the test setup will determine the mass and the friction values of the system and an experiment will be conducted with different cross-over frequencies to check when hunting occurs. Further, experiments will be done with the friction isolator in which the stroke and cross-over will be altered to check the hunting behavior and verify the simulations.

3.4 Design method

In this section, a design method for a friction isolator system will be proposed and used to realize a test setup. The test setup will be used to verify the design method.

After the implementation of the compliant joint is known, a step-by-step design method based on the parameters described in Section 3.3 can be initiated:

- Determine the desired and reachable cross-over frequency of the system, if this frequency is limited a friction isolator is useful. A higher possible cross-over frequency can mean hunting cycles do not occur in the system and the benefit of a friction isolator is limited.
- Determine the friction values of the bearing. If the difference between static and coulomb friction of the bearing is small, stick-slip might not occur and thus hunting cycles will not be an issue.
- From the static friction value, combined with the maximum stroke of the compliant joint, a drive stiffness can be determined. This drive stiffness is used to design the compliant joint, which should be designed such that the parasitic frequencies do not interfere with the desired cross-over frequency.
- Finally, the PID controller parameters can be determined when the mass of the system is known.

The steps will be discussed in greater detail in the remainder of this chapter.

3.4.1 Implementation of friction isolator

For the implementation of the compliant joint in the friction isolator, a parallel leafspring mechanism is chosen, of which a schematic overview can be seen in Figure 6. This type of mechanism has low stiffness in the moving direction and high stiffness in the supporting directions. At small displacements, the system will behave as a linear spring and the parasitic motion in height direction due to shortening is negligible. Further, this type of mechanism is relatively easy to implement and its behavior is predictable. Using SPACAR and analytical equations, the mechanism will be optimized to fit the application, which in this case means a low as possible drive stiffness, while the parasitic eigenfrequencies should be as high as possible.

As a starting point, the stroke of the flexures is set to 1mm from the neutral position to the end-stop in both directions. This size of stroke is estimated to be in the order of the displacements in a hunting cycle. Increasing the stroke would require the drive stiffness of the flexure mechanism to be lower, in order to keep the applied force at full stroke below the static friction of the bearing. A larger force would induce break-away of the cart, thus limiting the performance of the flexure mechanism. Both the flexure drive stiffness and the stroke of the flexures can be tuned to limit the required force for a full stroke.

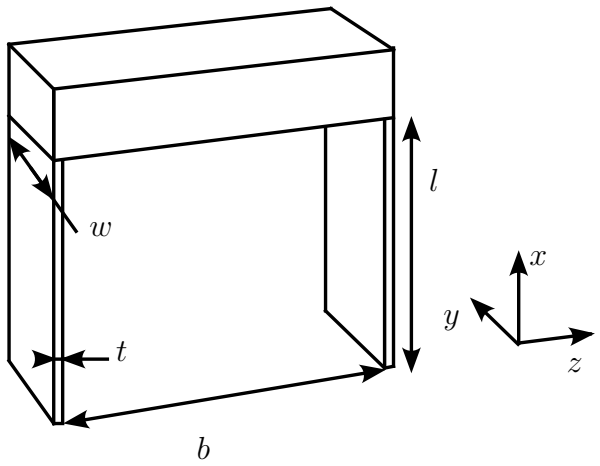

Figure 6: A schematic overview of a parallel leafspring mechanism. The direction of motion is the z-direction and the main dimension parameters are indicated.

The stiffness in the supporting directions of the compliant joint should be in the order of the support stiffness of the bearing so as to not limit the loading capacity. In order to reach the goal of a low drive stiffness while keeping the support stiffnesses high, either the length, l, should be increased or the thickness, t, decreased. These terms are present in cubed form in the analytical equations of the drive stiffness [23]. Increasing the length, however, will significantly decrease the stiffness in y-direction as well. Increasing the width, w, of the flexures yields more increase in support stiffness than in drive stiffness and is thus a viable option.

To find the optimal dimensions of the flexure mechanism, the finite element program SPACAR is used. Multiple possibilities will be analyzed in order to find the highest parasitic eigenfrequencies and thus the most optimal dimensions.

The actuation force has to be applied to the positioning stage, which is part of the compliant joint. The center of compliance of the mechanism is the most ideal point of actuation since no additional parasitic movements are introduced in the mechanism when actuated at this point. This point is however located in the center of the mechanism, which is impractical to apply the force. Therefore it is chosen to place the actuator underneath the flexure mechanism, such that the smallest additional reaction forces and moments are introduced.

3.4.2 Control

The system to be controlled contains 4 limit cases, which are identified in Section 3.1.2 and Table 1. Between these cases, the moving mass (and thus controlled mass) differs significantly, it is either only the mass of the flexure mechanism or the combined mass of the flexure mechanism and the cart. Since a single controller is used to control all cases, the controller should be stable and have satisfying performance in all cases. It was found that using the maximum mass for tuning the controller yields the best results, as is shown by Dong et al. [8].

In order to determine where the cross-over frequency should be placed, Bode plots of the four linearized cases are made and shown in Figure 7. In a single degree of freedom (DOF) system, the cross-over frequency should be placed after the first eigenfrequency of the system, in the mass-dominated region. In the current system, however, multiple DOF's are present which makes placing the cross-over frequency less straightforward. The figure shows that the behavior of the system changes significantly between the cases. When the cart is fixed through static friction in cases 1 and 3, it behaves as a spring in the low-frequency region. The stiffness in this region corresponds to the drive stiffness of the compliant joint or the pre-motion stiffness

in the LuGre friction model. In the case of a moving cart, the low-frequency behavior is mass dominated and at even lower frequencies the damper is dominant. In the systems where the flexure mechanism moves freely (cases 1 and 2), an eigenfrequency is found around 10 Hz. In the case of both masses moving, this leads to an anti-resonance and a resonance frequency, as is seen in the blue line. Further up the frequency band a difference in mass lines can be seen between the sticking and slipping systems, since the moving mass differs. For all systems, the internal parasitic frequency is found around 300 Hz. When the compliant joint is pushing the stroke limiters (cases 3 and 4), another anti-resonance and resonance frequency pair is found just after this parasitic frequency.

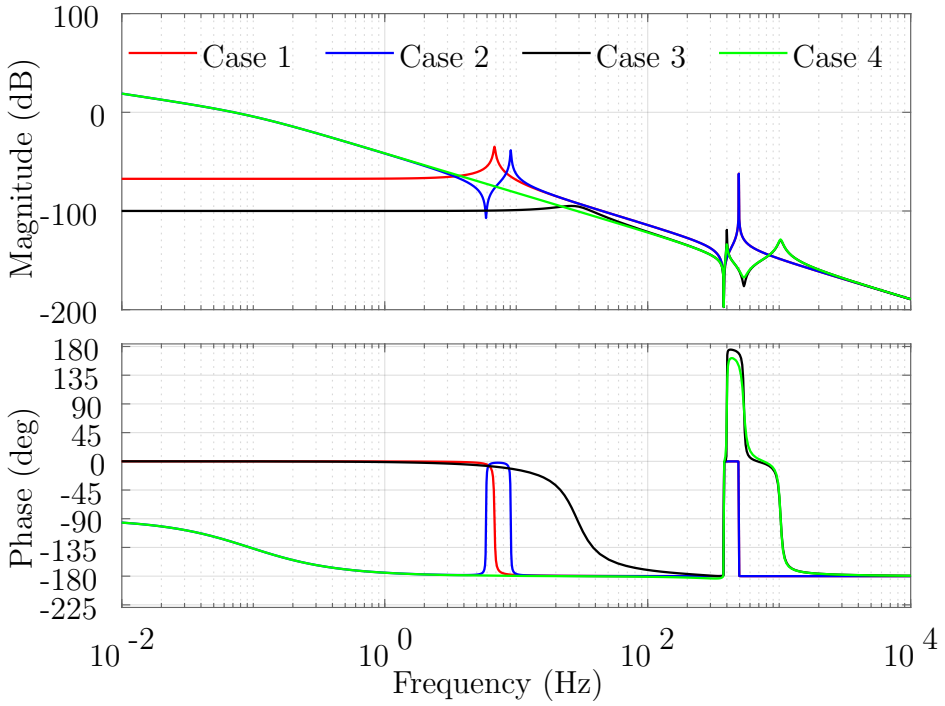

Figure 7: Bode plots of the plant, with control force as input and the position of the end-effector as output of the different limit cases the plant can be in. These cases correspond to the cases identified in Section 3.1.2.

A stable controlled system would either require a cross-over frequency significantly smaller than the first eigenfrequency or significantly larger than this frequency. The lower cross-over frequency leads to lower control forces however, this also decreases the performance. Settling times are shortened significantly with a higher cross-over frequency. Since the controller will be tuned on the non-isolated system, state 3 and 4 from Figure 7 are mainly taken into account. The cross-over frequency should be chosen such that the magnitude crosses the 0 dB line only once for stability purposes. At this cross-over point, the phase angle should be above -180 °.

Another important factor in placing the cross-over frequency is the influence on the hunting behavior. Since the cross-over frequency determines the bandwidth of the system, it can be tuned such that the hunting behavior is mitigated. For the sake of this research, however, the cross-over frequency will thus be tuned to a region in which the system will still show hunting.

In Figure 8 the bode plots of the complete controlled system from error to output position, with different prescribed velocities of the cart are shown. This shows how the low-frequency behavior of the system changes due to changes in the friction force, which affects the gain cross-over point as well. However, with each of these cross-overs the system is stable. The cross-over

frequency is tuned to 8 Hz such that hunting occurs. The cross-over frequency can be tuned to up to 60 Hz, using the discussed design method. This does increase the performance of the system, however, also defeats the purpose of this research since hunting does not occur with this cross-over frequency.

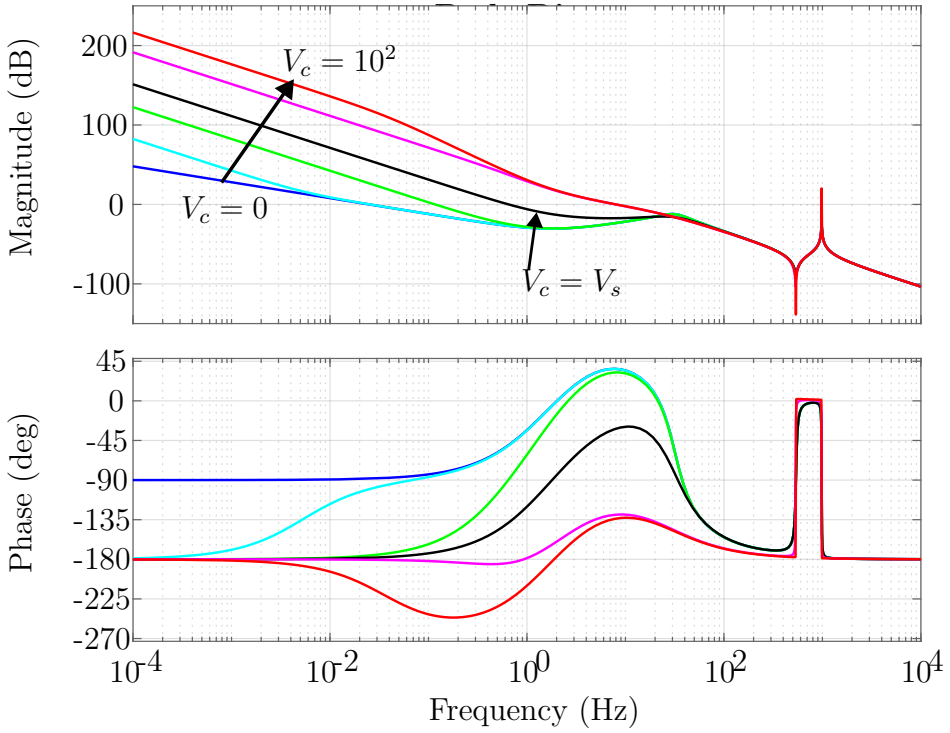

Figure 8: Open loop Bode plot of the controlled friction isolator with stroke limiters and increasing initial bearing stage speed, such that the low frequency behavior changes due to LuGre changes.

A stability check on the system is performed by linearization of the different states in the system and analyzing each independent state. The gain and phase margin are taken into account as well as the poles. This check is not a definite check, but it does give insight into how the system will respond. Together with the system behavior in the simulations, an assumption can be made on the stability of the system.

3.5 Realization of test setup

The design of the test setup that is used in this research is discussed in depth in this section. The setup is designed to test the performance of the friction isolator and verify the parameter study. The setup is designed as modular as possible, such that the dimensions of the leafsprings can be altered if required for test purposes. Further, the compliant joint can be fixed such that the comparisons can be made between the isolated and non-isolated case. An overview picture of the setup can be seen in Figure 9 and an overview of the main components in the setup can be seen in Figure 10.

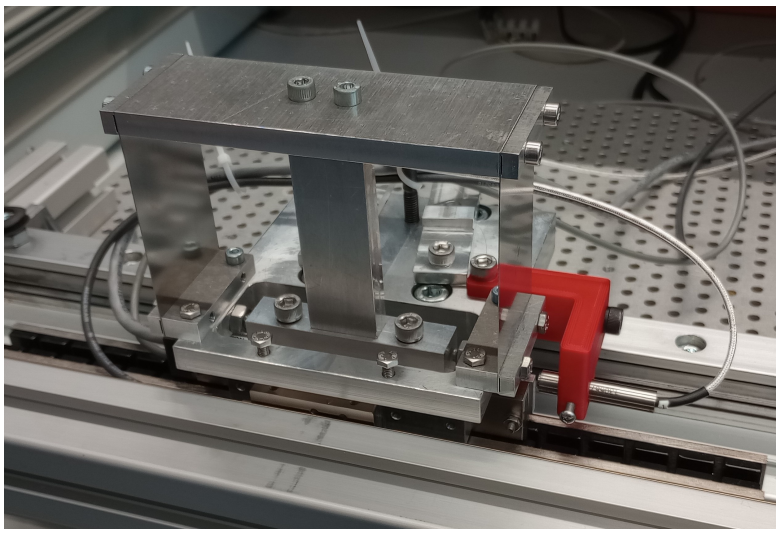

Figure 9: Overview of the test setup. The system shown is the friction isolator system since the fixtures are not used to fix the compliant joint.

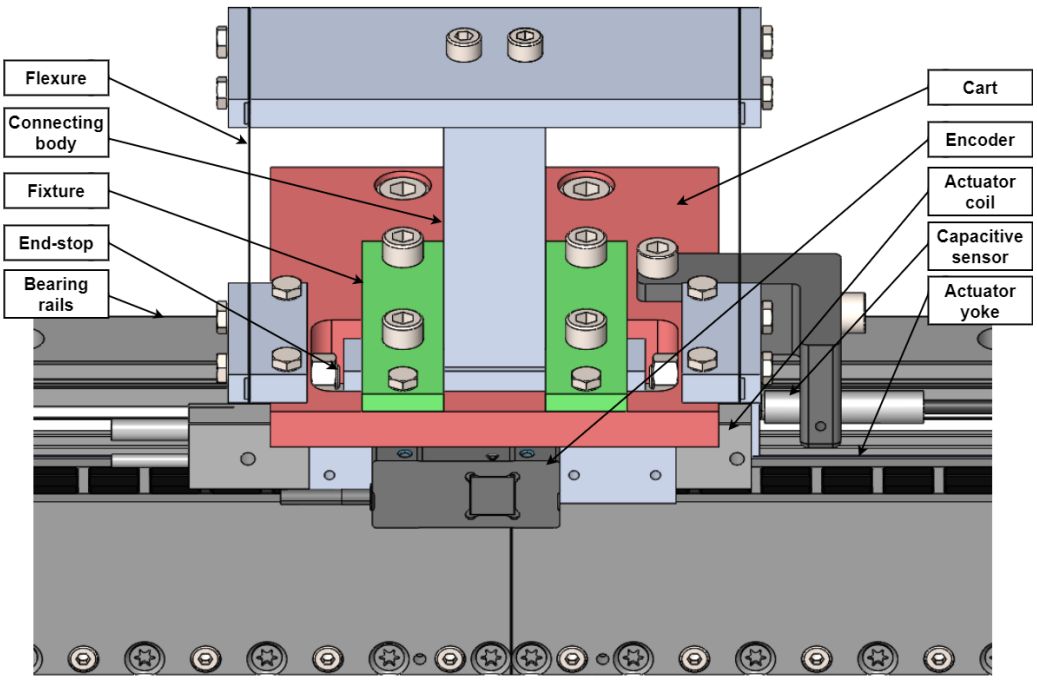

Figure 10: CAD design of the test setup, with the main elements highlighted. The shown system is the non-isolated system. Note, the linear scale of the encoder is not shown in this picture for clarity.

The basis of the test setup is a linear guide of type Franke FDA25, with a rail length of 400 mm and needle bearings that allow for motion. The motion is provided by a Technotion UM6 linear ironless actuator, which is chosen because this type of actuator is not affected by cogging. This leads to a more constant force application compared to an iron core actuator, which makes it more suitable for high-precision positioning. The Technotion UM6N coil is combined with two 150 mm magnet yokes, such that a stroke of approximately 160 mm can be made. This actuator has a peak force of 200 N, as a result of which the system can reach accelerations close to 10 G. The actuator is mounted directly to the compliant joint through the connecting body.

An Etel AccurET 400 10/20A motor controller is used to power the actuator and run the PID controller. This unit gets position feedback from a Heidenhain LIC4119 absolute linear encoder at a sample time of 50 μs and a resolution of 1 nm. The position control is done in real-time on the Etel AccurET controller. The encoder is mounted as close to the actuator as possible, to minimize parasitic motions.

A Lion precision C8-3.2 capacitive sensor is mounted to measure the displacement of the flexure mechanism relative to the cart. This sensor is combined with a cpl290 driver, to obtain a RMS resolution of 30 nm. These measurements will be used to determine the force applied to the bearing and study the behavior of the compliant joint during motion.

The compliant joint is implemented through a parallel leafspring mechanism. The dimensions of the leafsprings are determined to be $70 \times 45 \times 0.35$ mm, length, width, and thickness respectively. SPACAR simulations show this mechanism has a drive stiffness of 2.4 N/mm and a first eigenfrequency of 11 Hz. The first parasitic frequency is found around 360 Hz and the stress is determined to be maximum 50 MPa at a deflection of 1 mm. The leafsprings are made of stainless steel.

Stroke limiters are implemented in the compliant joint by means of a bolt and a locking nut, such that the stroke of the joint can be altered for testing purposes.

3.6 Test plan

The test setup will be used to verify the design method and the simulations of the parameter study. To verify the masses and control parameters, the setup is identified by establishing Bode plots. The stiffnesses and friction values can be identified by applying a motion profile to the system and analyzing the position and force signals from the position controller. To check whether the hunting behavior is indeed mitigated by the friction isolator, experiments similar to the simulations will be conducted. Further, experiments will be conducted to verify the simulations. The non-isolated system will be tested at different cross-over frequencies to check the influence of this parameter. The friction isolator will be tested with different stroke lengths and varying cross-over frequencies.

Another experiment will be conducted to analyze the in-position stability of both systems. Due to the lack of damping in the compliant joint, the in-position stability might be diminished compared to the non-isolated case.

4 Results

4.1 Results of parameter study

In this section the results of the parameter study as described in Section 3.3 will be discussed. The results can be seen in Figures 11 till 15. In all figures, a marker is plotted which highlights the chosen values of the parameters that are used in the other simulations.

Path and system parameters Figure 11 shows the results of varying the path and the cross-over frequency and mass of the system. The cross-over frequency and mass of the system both affect the control parameters and the performance of the system and are thus combined in this simulation. The path is in this case defined by an acceleration value and the time of acceleration, which equates to the traveled length. From the figure, it becomes clear that changing the traveled path is not a robust solution against hunting behavior. It seems as if

there is an inverse relation with the acceleration time, above which a stable amount of hunting cycles is always present.

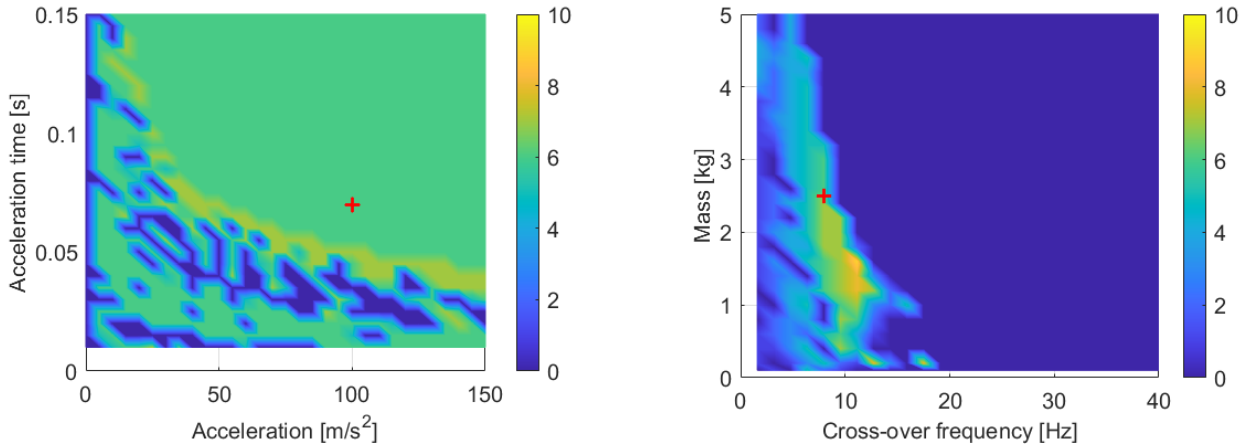

Figure 11: A) Resulting amount of hunting cycles according to the metric by altering the acceleration value and acceleration time. B) Resulting amount of hunting cycles according to the metric by altering the cross-over frequency and mass. The red marker indicates the evaluation point for the other studies.

In Figure 11 B, it can be seen that with a higher cross-over frequency, larger than around 20 Hz in this case, no hunting occurs. With a higher cross-over frequency, the controller responds faster which can prevent hunting cycles from occurring.

Increasing the mass while keeping the cross-over frequency fixed, can terminate hunting as well. The controller gains are adjusted for the larger mass, such that the initial response to a prescribed motion is not changed. The difference is found after the bearing is affected by stiction after the initial overshoot. This difference can be explained by the larger inertia of the moving stage. According to Newton's second law, the acceleration of a mass is lower if the mass is larger and the applied force is kept equal. This is the case in this situation, the force applied to the cart at the instance of breakaway is equal to the difference between the static and dynamic friction force. This force is equal for all simulations in this study. When this force is applied to a larger mass, the acceleration is smaller, and therefore the overshoot of the reference position is smaller as well. This slows down the build-up rate of the integral action. With the same control bandwidth, this also means that the proportional gain can be adjusted with the slowly decreasing error as the bearing moves in the pre-sliding regime. This leads to an even slower increase in the total control force and slowly increases the movement of the bearing. Abrupt breakaway does however not occur and the system settles to the desired position.

Friction forces and control parameters In Figure 12 A, it can be seen that the static friction force has to be significantly larger than the Coulomb friction force in order for hunting to occur. This is logically explained by the stick-slip conditions, in which the static friction has to be larger than the dynamic friction. A larger gap between the static and Coulomb friction force leads to more hunting cycles. At the point of breakaway of the bearing, the control force is therefore also significantly larger than the dynamic friction force resulting in a larger overshoot. Due to a larger error, the proportional part of the controller generates a larger force and the build-up rate of the integral action is increased as well. This results in the breakaway force being reached sooner. In Figure 13, the individual actions of the PID controller are plotted

during hunting. In the top graph, $F_c = 0.5$ and $F_s = 4$, and in the bottom graph $F_c = 1.5$, while keeping F_s equal thus creating a smaller gap in static and dynamic force for the bottom graph. It can be seen that the controller requires more time to reach the breakaway force since the integral action is responsible for a larger part of the force.

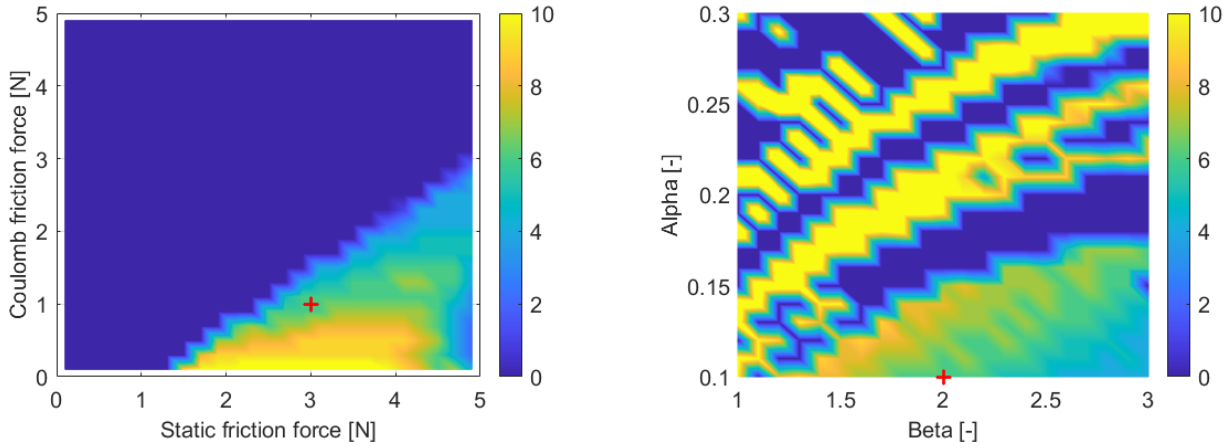

Figure 12: A) Amount of hunting cycles according to the metric by altering the static and Coulomb friction forces. B) Amount of hunting cycles according to the metric by altering the controller parameters α and β. The red marker indicates the evaluation point for the other studies.

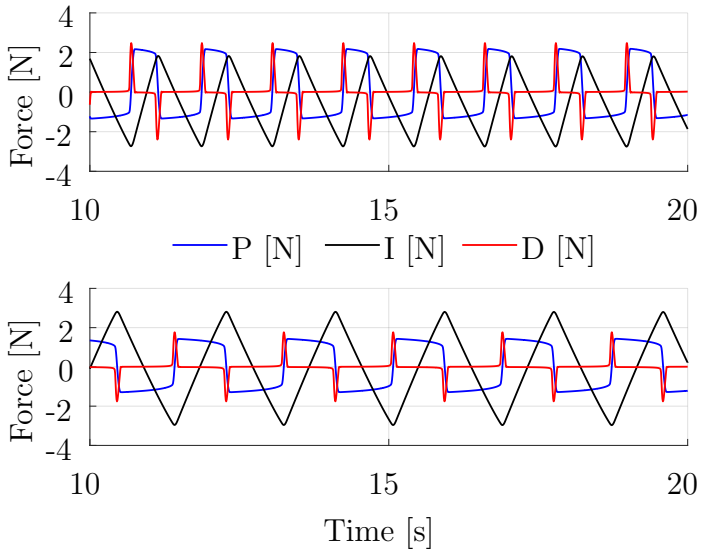

Figure 13: Behavior of PID actions during hunting cycles. In the top graph $F_c = 0.5$ and $F_s = 4$, while in the bottom graph $F_c = 1.5$ and $F_s = 4$.

For increasing values of β a trend of a smaller amount of hunting cycles can be seen in Figure 12 B. This trend can be expected from the defining equation of the PID controller. Since β is only related to the integrator action of the controller, it will affect the reaction time to a steady state error. A larger value of β leads to a smaller integrator gain and thus slowing down the reaction. α increases the proportional gain of the controller, therefore resulting in a larger control force. This means the integral action does not need to build up as much force, and thus the breakaway force of the bearing is reached sooner. A trend can be seen in the figure that larger values of α lead to more hunting cycles, due to the faster response.

Overall, these two parameters do not give a robust combination to mitigate hunting cycles and thus the determination of these parameters will mainly be based on the stability of the controller.

Friction isolator stiffness and damping Figure 14 shows variations in the parameters of the friction isolator. The first figure shows that the stiffness of the compliant joint is limited in order for the isolator to work. This is to be expected when taking the principle of the friction isolator into account. At a smaller allowed stroke of the compliant joint, the stiffness of the joint can be higher, since the force applied to the bearing at the maximum stroke is then still smaller than the static friction force. A stroke of 0 mm effectively turns the friction isolator into the non-isolated system and thus hunting cycles are present at this stroke.

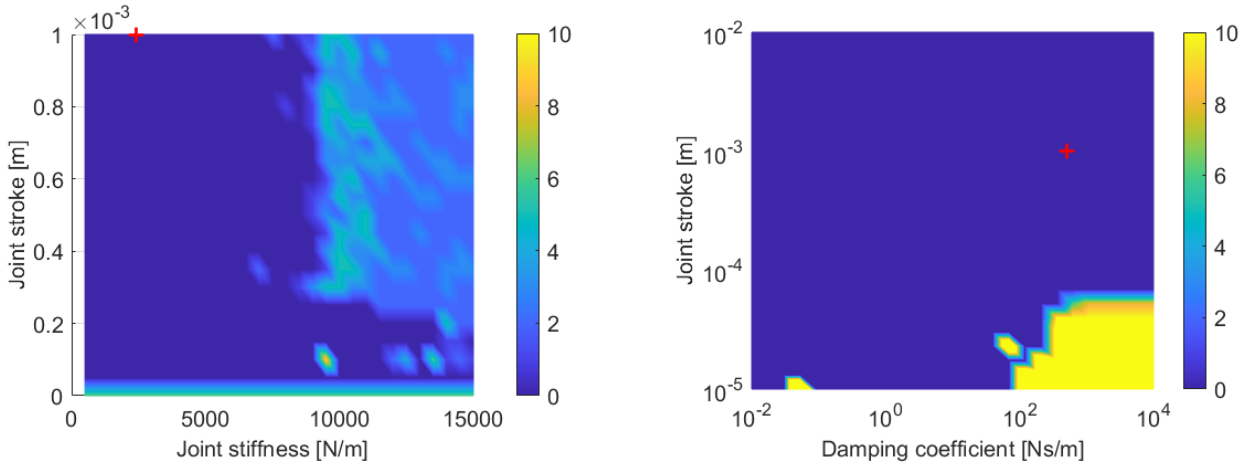

Figure 14: A) Resulting amount of hunting cycles according to the metric by altering the stroke and drive stiffness of the compliant joint. B) Resulting amount of hunting cycles according to the metric by altering the compliant joint stroke and the damping coefficient of the stroke limiters. The red marker indicates the evaluation point for the other studies.

When larger damping is present in the stroke limiters of the friction isolator, the stroke has a minimum value of around 0.1 millimeters for the friction isolator to be effective, as can be seen in Figure 14 B. Thus the contact between the compliant joint and the stroke limiter affects the hunting behavior. On the other hand, from this study it can be seen that the required stroke of the compliant joint is significantly smaller than the amplitude of a hunting cycle. The compliant joint is thus used to overcome the irregularities introduced by the friction, rather than positioning over the full range of a hunting cycle, while the bearing is fixed by static friction.

Friction isolator mass and friction forces From Figure 15, it can be seen that the ratio between the mass of the positioning stage and the mass of the bearing cart does not have a significant impact on the working principle of the isolator. For a working friction isolator, the coulomb and static friction force do not lead to hunting cycles in the isolated stage as expected.

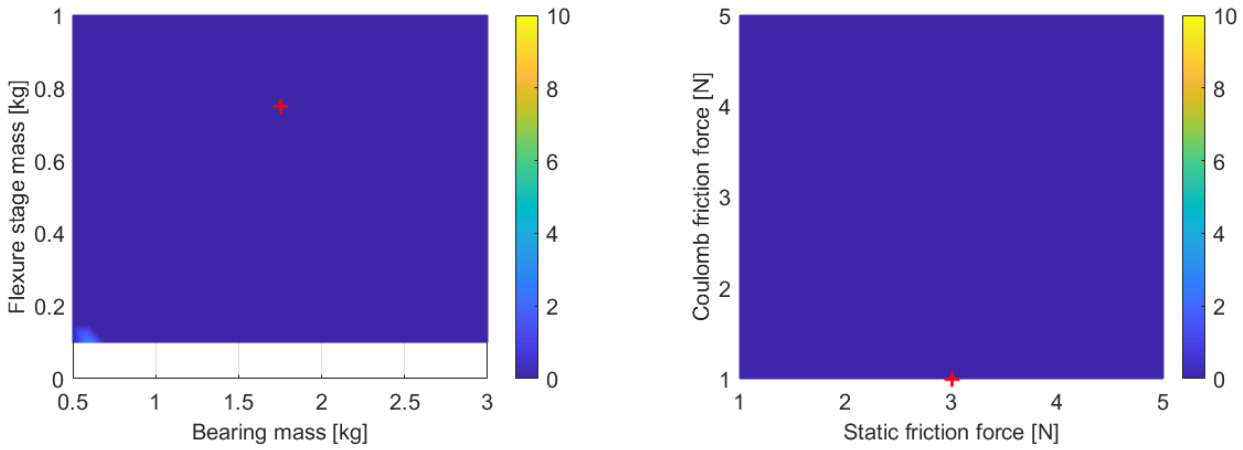

Figure 15: A) Resulting amount of hunting cycles according to the metric by altering the masses of the bearing and compliant stages. B) Resulting amount of hunting cycles according to the metric by altering the friction forces in the friction isolated system. The red marker indicates the evaluation point for the other studies.

Friction isolator cross-over Lastly, a study is performed on a grid varying the stroke of the compliant joint and the cross-over frequency of which the results can be seen in Figure 16. From this study it is found that the cross-over frequency also affects the hunting behavior of the friction isolator system. At smaller cross-over frequencies, hunting can still occur even in the isolated system. The boundary values of the cross-over frequency below which hunting occurs is affected by the stiffness of the compliant joint. A lower drive stiffness lowers the cross-over frequency at which hunting occurs. This can be explained by the working principle of the friction isolator.

This study also shows that the stroke of the compliant joint is not required to be a similar size to the amplitude of the hunting cycles. Above a certain stroke, the boundary of the cross-over frequency does not change.

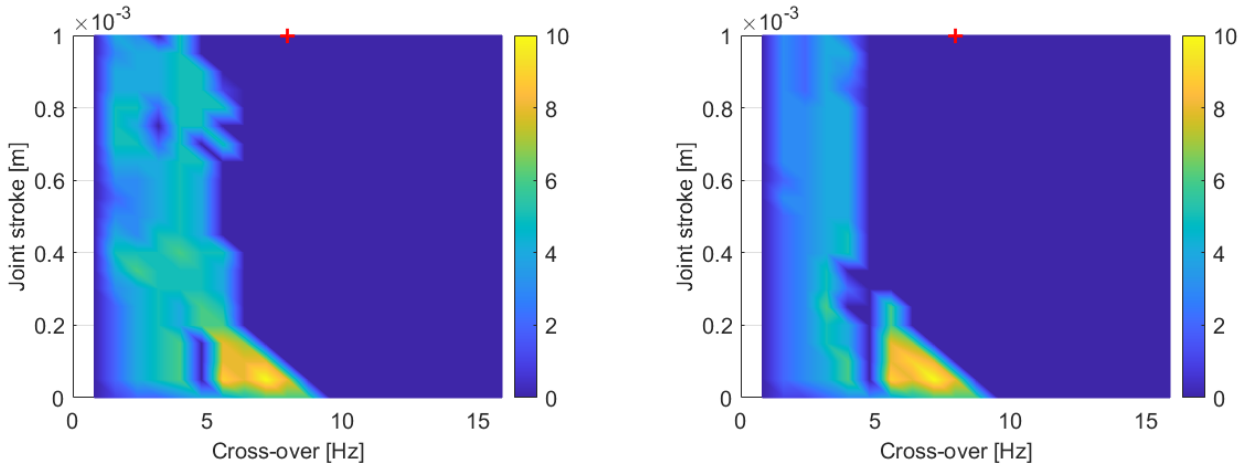

Figure 16: A) Resulting amount of hunting cycles by altering the compliant joint stroke and cross-over frequency. B) Results of the same study, but with a lower drive stiffness of the joint. $k_j = 1 * 10^3 N/m$ instead of $k_j = 2.4 * 10^3 N/m$.

4.2 Setup identification

In this section, the identification of the experimental setup will be discussed. Bode plots are used to determine the mass and control parameters. The friction forces and the drive stiffness of the compliant joint are determined from the position and force signals from the Etel AccurET position controller and the capacitive sensor.

4.2.1 Mass

To determine the right controller parameters, the moving mass of the system is required. Therefore, this mass needs to be identified in the real setup, such that the controller parameters can be fitted to the real system. Bode plots have been made of the mechanical plant for both the friction isolator and the non-isolated system. In Figure 17, the averaged Bode plot from ten identifications of the non-isolated system is shown, in which a mass line is clearly visible. An average value is taken since each individual identification shows some noise at a frequency range from 10 Hz up to 80 Hz, which can still be seen in the phase angle. All identifications can be seen in Appendix A.1. The result of the mass line fit is plotted in Figure 17, which equates to a mass of 2.5 kg. This is larger than the weighed value of 1.7 kg for the complete system. This mass is a combination of 1.2 kg for the bearing cart and 0.5 kg for the flexure stage, including actuator coils and the encoder head. Factors that add to this difference in mass are the cables that move with the system and the motor force constant that might vary from the datasheet of the actuator. This constant is used in creating the Bode plot and the line could thus be shifted somewhat. The control parameters are calculated using the same motor force constant, such that this parameter is eventually not affecting the control system.

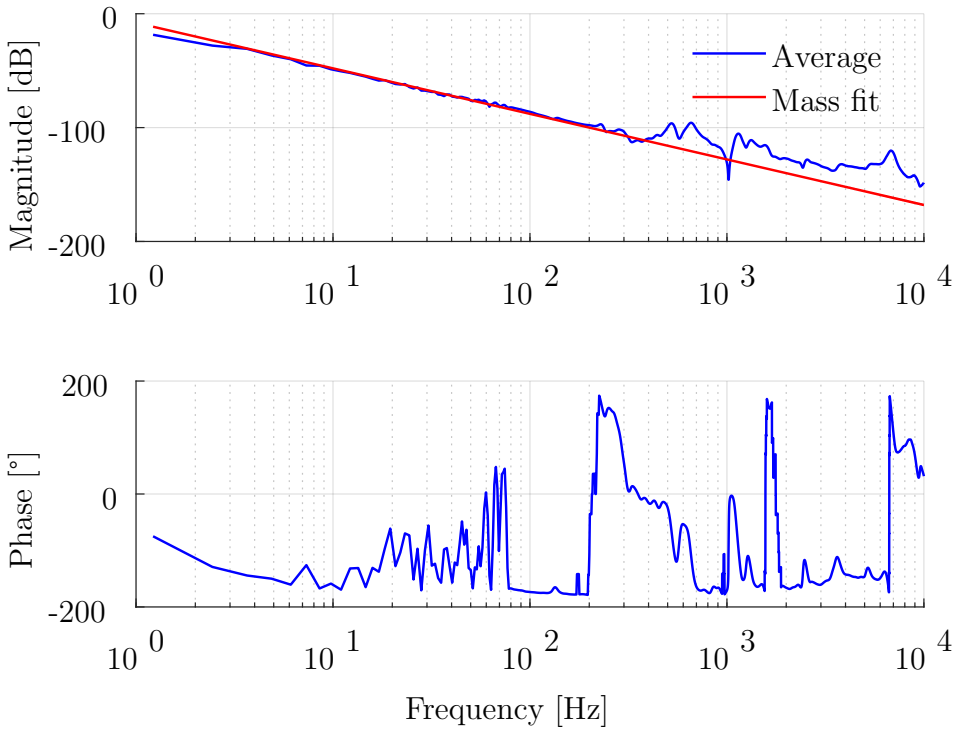

Figure 17: Experimental open loop Bode plot of the mechanical plant of the non-isolated system, averaged from 10 identifications. The mass line can clearly be seen up to around 200 Hz, which is fitted to determine the value of the mass.

Identification of the friction isolator is done to identify the moving mass of the complaint joint

and the positioning stage. The resulting Bode plot can be seen in Figure 18, in which it should be noted that this is an individual identification and not an averaged plot like for the non-isolated system. The bearing cart is freely moving in this identification and the stroke limiters are set to the maximum stroke of 8 mm, for safety reasons. The first natural frequency of the flexure mechanism coincides with the calculated value of 11 Hz, the first parasitic frequency is found at a lower frequency value than expected around 300 Hz. Between these frequencies, the mass line is fitted, which equates to a moving mass of 0.75 kg.

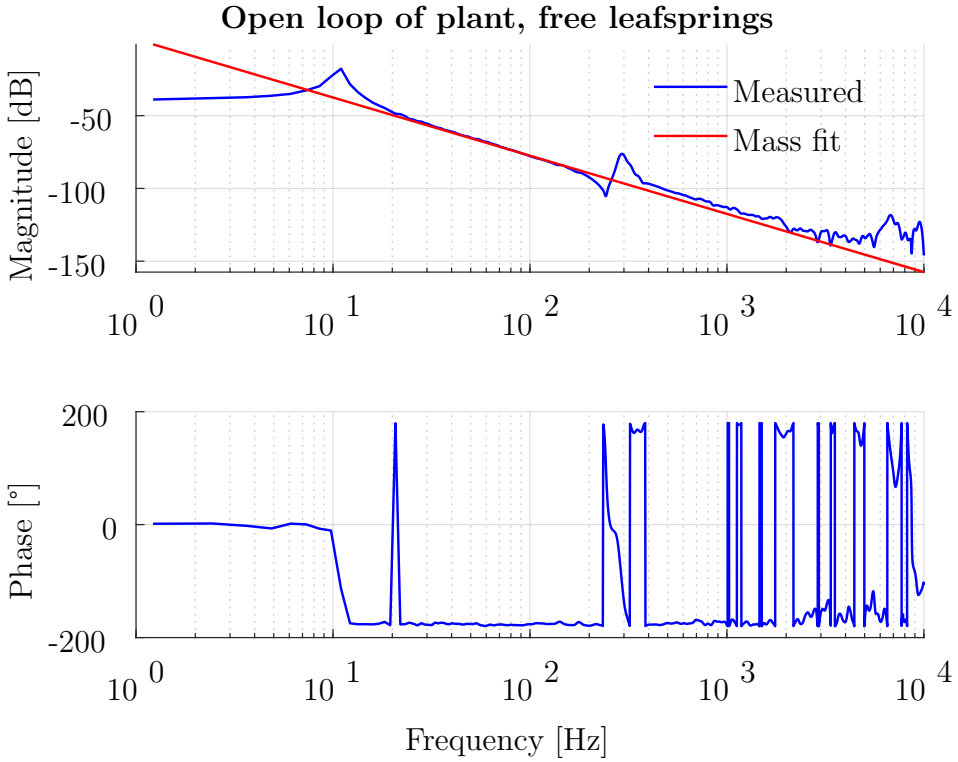

Figure 18: Experimental open loop Bode plot of the mechanical plant of the friction isolator, in which the mass line is fitted to determine the value of the mass. Note, the stroke limiters are set to the maximum stroke of 8 mm in this case.

4.2.2 Stiffness

To determine the drive stiffness of the compliant joint, the bearing cart is fixed to the rail and the end effector is moved in steps of 0.3 mm. Deflections of the compliant joint fully account for the displacements of the positioning stage. The force readout of the Etel AccurET controller is used. In Figure 19, the resulting position and force signal of the test can be seen. The force signal is filtered by means of a lowpass filter with a cut-off frequency of 25 Hz and smoothed using the `smooth` function in Matlab. For calculating the stiffness, an averaged value over the time the stage has settled is used.

Since the applied force is not zero in the undeflected state of the compliant joint, the difference between the applied force in the position steps is used. The stiffness is determined to be $2.9 \cdot 10^3$ N/m, which is $0.5 \cdot 10^3$ N/m larger than the value calculated value from SPACAR. This difference can be explained by the cables that are attached to the actuator and encoder, as well as the motor force constant. Possible misalignments in the mounting of the leafsprings can be a factor in this difference as well.

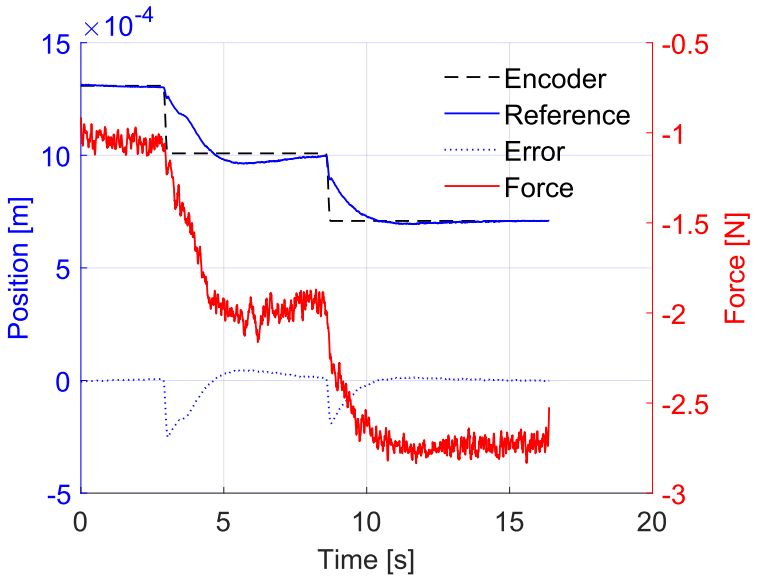

Figure 19: Results of the experiment to determine the stiffness of the compliant joint. The cart is fixed and the measured position is thus the deflection of the compliant joint. The force is measured by the AccurET controller.

4.2.3 Friction

Experiments have been conducted to determine the level of static friction in the bearing. Due to limitations of the AccurET controller, prescribing a reference force to the actuator is not possible. A motion profile with standstill and constant velocities is prescribed to the friction isolator, such that the bearing will both stick and slip during the movement. Using the deflection of the compliant joint, the applied force can be determined.

Figure 20 contains the results of one of the friction identification tests. The reference path and encoder readout can be seen, as well as the readout from the capacitive sensor containing the relative position of the stage with respect to the bearing cart. Further, the velocity signal of the bearing cart is seen as well. This signal clearly shows stick-slip behavior, with several spikes in the velocity. These spikes are preceded by peaks in the relative position signal, thus meaning the compliant joint deflects while the bearing is sticking and then suddenly starts moving, resulting in a spike in the velocity signal. From multiple experiments, the static friction is determined to be in the range of 1 to 2.5 N.

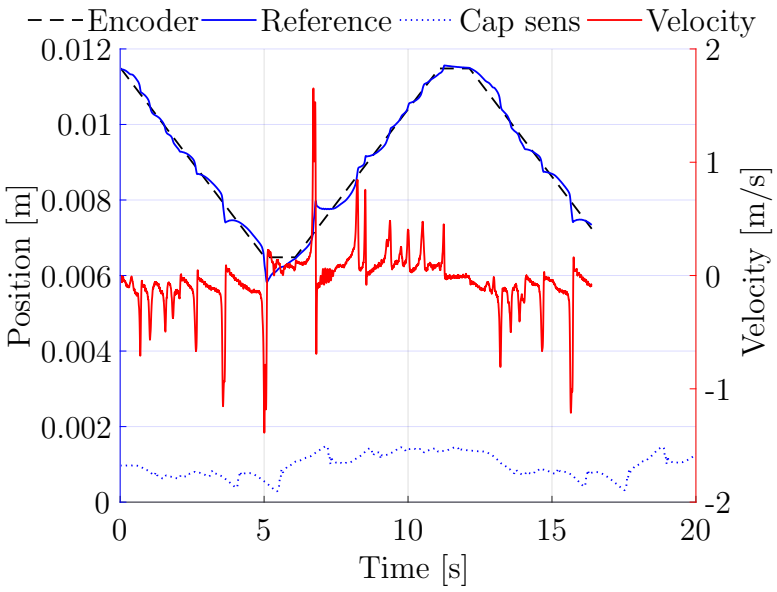

Figure 20: Typical example of an experiment to determine the static friction in the bearing. The reference position and measured position from the encoder are shown, as well as the relative position signal from the capacitive sensor and the velocity of the encoder.

Identifying the Coulomb friction is tried by moving the bearing with a constant velocity over a long range of 150 mm. Reading out the applied force should give insight into the dynamic friction of the bearing. In Figure 21, the results of two experiments can be seen at velocities of $2.5 \cdot 10^{-3}$ m/s and $10 \cdot 10^{-3}$m/s. It can be seen however, that the applied force in both cases shows oscillatory behavior, which is position dependent. From these experiments, no conclusions can be drawn on the dynamic friction force and it shows how unpredictable the friction can be in a real setup.

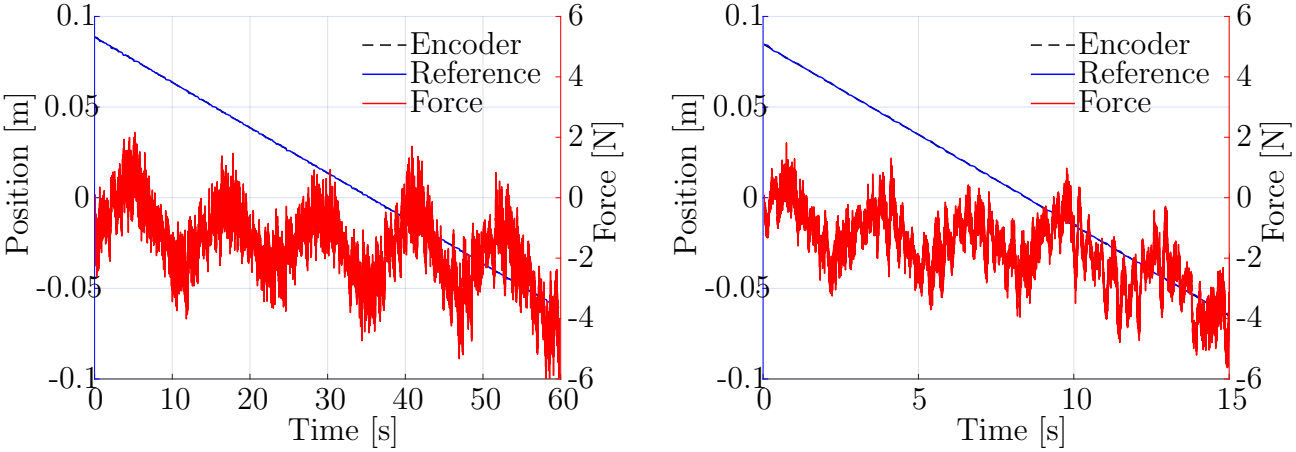

Figure 21: Applied force over a constant velocity motion with a length of 150 mm. Velocities of $2.5 \cdot 10^{-3}$ m/s and $10 \cdot 10^{-3}$m/s are used in the shown experiments. The applied force shows position dependent oscillations.

4.2.4 Control

Verification of the controller is done through experimental open loop Bode plots of the controlled system. The main parameter to look at is the location of the cross-over frequency. In Figure 22, identifications of the non-isolated case can be seen with increasing cross-over frequency of

the controller. It can be seen that the Bode plots cross the 0 dB line approximately at the intended cross-over frequency. Further, it can be seen that a risk of instability arises at the highest cross-over, where another zero dB line crossing can be found around 600 Hz.

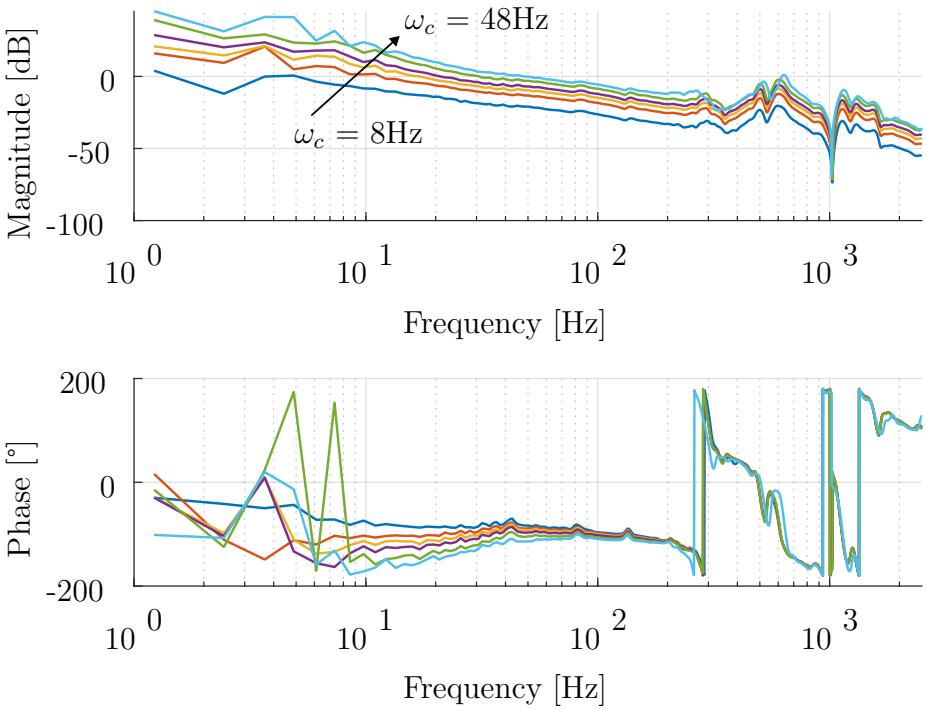

Figure 22: Experimental open loop Bode plot of the controlled system for the non-isolated case. The cross-over frequency of the controller is varied from 8 to 48 Hz (or 50 to 300 rad/s). The crossings of the 0dB line coincide approximately with the intended locations.

An identification of the controlled system has been performed for the system with the friction isolator as well, of which the open loop Bode plot can be seen in Figure 23. The controller has been set to a cross-over frequency of 8 Hz in this case. The actual crossing of the 0 dB line is however found around 20 Hz, which can be explained due to the controller being designed for a larger moving mass. For the friction isolator, the cross-over frequency of 48 Hz was found to be the highest stable frequency. Tuning the controller to a higher cross-over leads to resonances in the compliant joint.

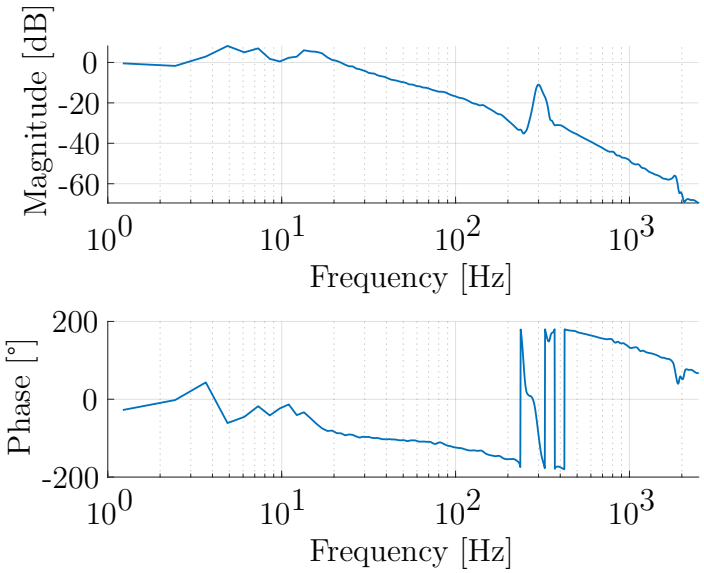

Figure 23: Experimental open loop Bode plot of the controlled system for the friction isolator. The cross-over is set at 8 Hz, though the actual crossing is found at 20 Hz.

4.3 Verification by test setup

The working principle of the test setup is verified by experiments conducted on the test setup. Further, experiments are performed to verify the parameter study. The results of the experiments are discussed in this section.

4.3.1 Control

As stated in Section 4.2.4, the controller applied to the test setup is verified with the controller used in the simulations. The system behaves stable, up to a cross-over frequency of 48 Hz. Above that, parasitic resonance frequencies are reached and unstable resonances can occur. These resonances are not only found in the compliant joint but in the frame holding the linear scale of the encoder as well.

4.3.2 Hunting experiments

The friction isolator is tested for its ability to mitigate the hunting effect. Figure 24 shows a typical result of moving the setup over 100 mm, with a prescribed acceleration of 100 m/s^2. Results of both the isolated and non-isolated system are plotted in this graph, from which it can be seen that hunting cycles are present in the non-isolated system, while the friction isolator settles to the reference position.

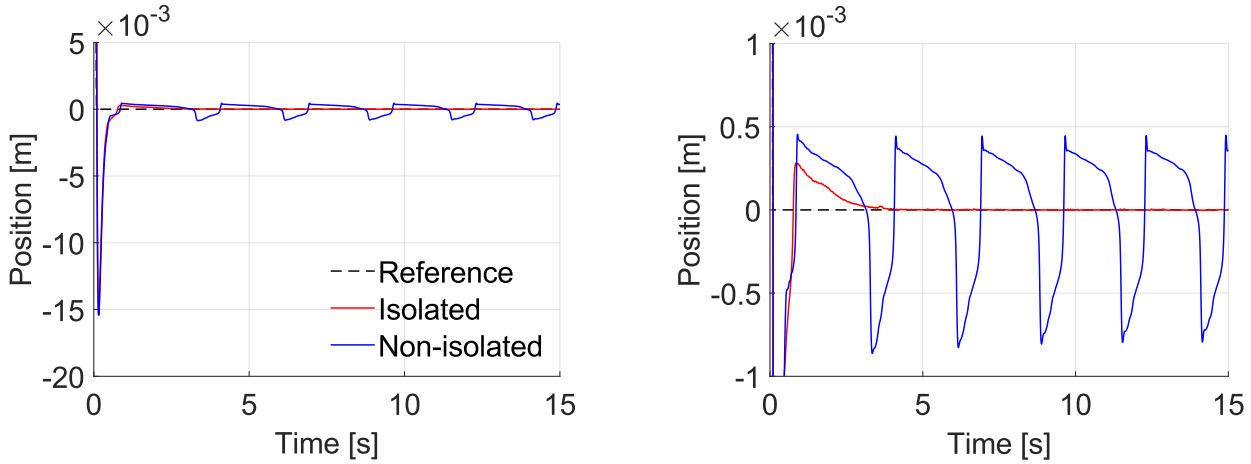

Figure 24: A) Postion data of the isolated and non-isolated system after applying a 100 mm step movement, with a prescribed acceleration of 100m/s^2, at a controller cross-over frequency of 8Hz. Hunting cycles can be seen for the non-isolated system, while the isolated system settles to the reference position. B) The same graph with a zoomed in position scale.

The same motion has been prescribed to the non-isolated system for varying cross-over frequencies. The results of these experiments can be seen in Figure 25. This experiment shows how the increasing cross-over frequency increases the performance of the system, since the response time to errors becomes smaller and the overshoot in the hunting cycles decreases. As expected from the parameter study, with increasing cross-over frequency the hunting cycles eventually are mitigated. Though the required cross-over frequency to mitigate the hunting behavior is found to be 14.3 Hz in this experiment, whereas in the parameter study a lower frequency is sufficient. This can be explained by the friction model not being exactly identified. It can be seen from the figure as well, that no hunting occurs at the cross-over frequency of 9.5 Hz, though hunting cycles can be initiated at this frequency.

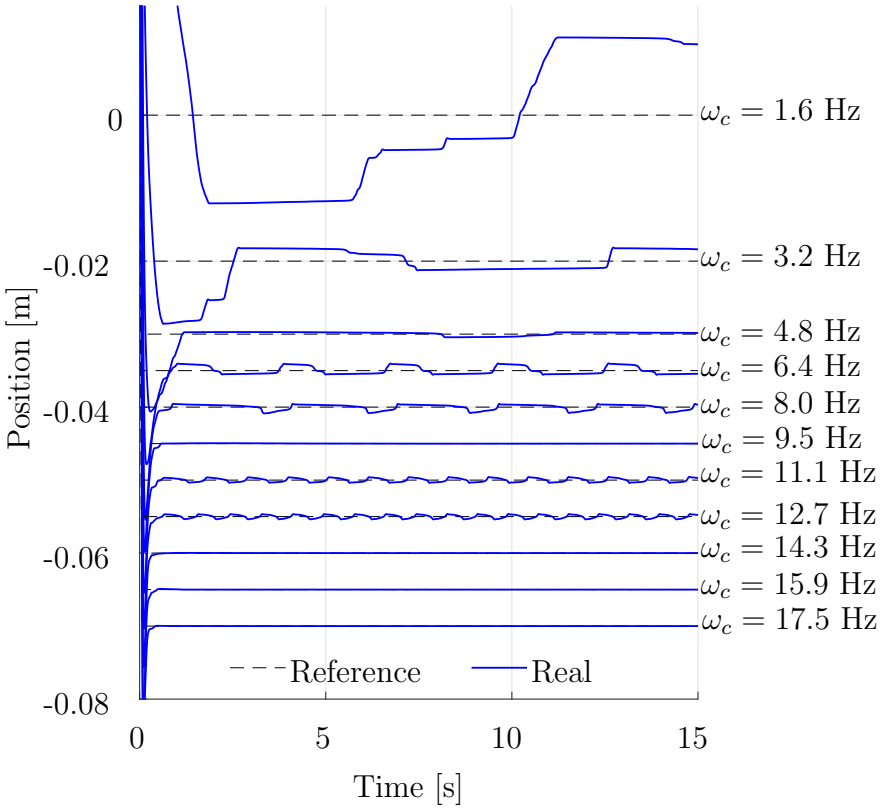

Figure 25: Resulting positions for varying cross-over frequency for the non-isolated system after an applied step motion of 100 mm, with 100 m/s^2 acceleration.

Joint stroke and cross-over frequency variation

The stroke of the compliant joint and the cross-over frequency of the controller have been altered for experiments on the test setup. The results of this experiment can be found in Figure 26. In this figure the number of hunting cycles according to the metric set in Section 3.2.2 are plotted for the different parameter values. It can be seen that at higher cross-over values, hunting is not present in the system at all. The trend is similar to the trend seen in the friction isolator cross-over parameter study.

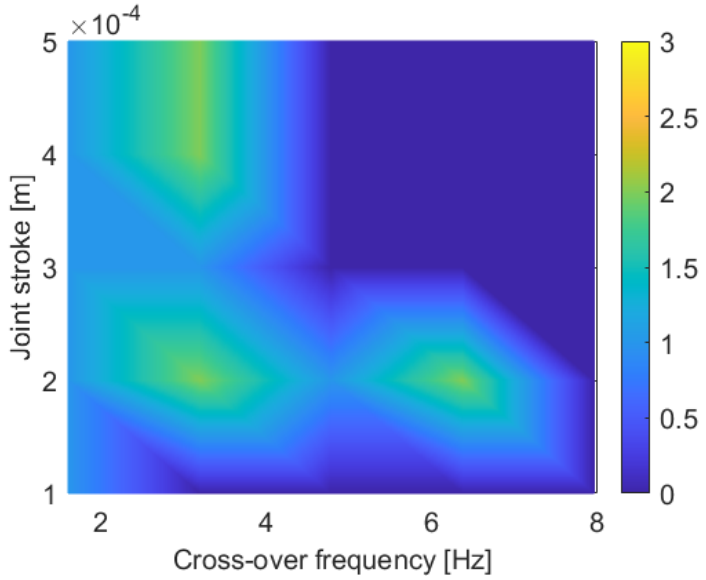

Figure 26: Resulting amount of hunting cycles after varying the stroke and cross-over parameters on the test setup.

Comparison with simulated hunting cycles

In order to verify the simulation of the hunting cycles, a comparison is made between the hunting cycles seen in the test setup and the simulated cycles. In Figure 27, the comparison can be seen for the non-isolated system that is tuned to a cross-over frequency of 8 Hz. The amplitude of the cycles is similar, but the frequency of the simulated hunting cycles is almost double the frequency of the cycles in the real setup. Further, the cycles in the simulation are symmetric, while the cycles in the real setup show more variation. This can be explained by the friction forces in the bearing in the real setup not being even over the whole length of the rail.

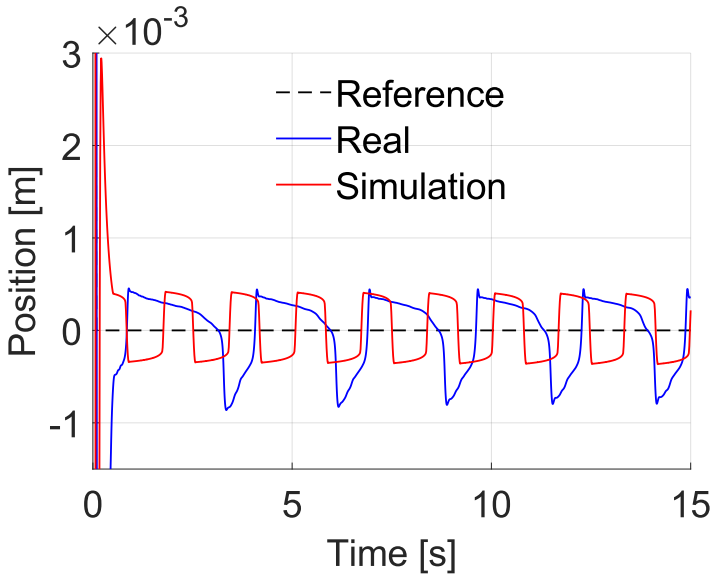

Figure 27: Comparison of the hunting cycles seen in the real setup and the simulated hunting cycles. The same motion is prescribed to both systems and the cross-over is set at 8Hz.

In-position stability

One of the drawbacks of the friction isolator can be found in the diminished in-position stability that is diminished. A comparison is made between the isolated and non-isolated system regarding the stability when the system is settled, of which the results can be seen in Figure 28. Both systems are tuned with a cross-over frequency of 16 Hz in this experiment and the position defers a maximum of 0.1 μm for the non-isolated system. For the system with the friction isolator, more deviation to the reference can be seen, up to 1 μm. This phenomenon can be explained by the lack of damping in the compliant joint, which is present in the non-isolated system through friction forces.

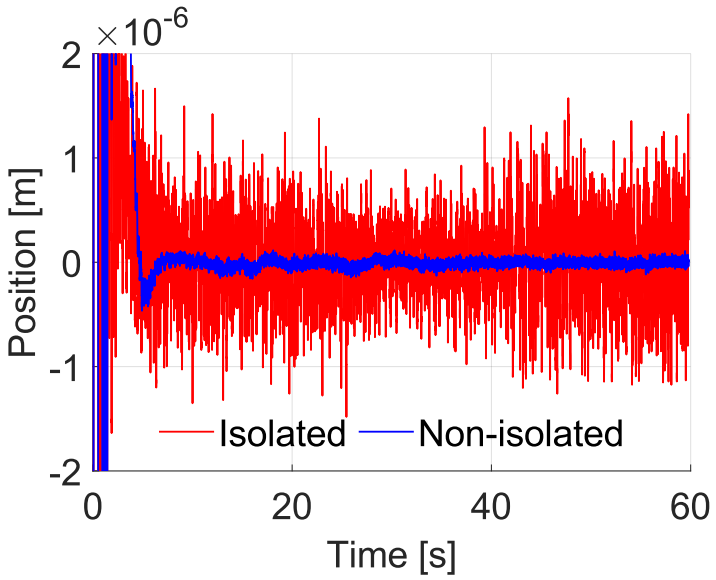

Figure 28: In position stability comparison between the isolated and non-isolated system. Both systems are tuned to a cross-over frequency of 16 Hz.

4.3.3 Design method

Through the experiments done with the test setup, the design method is verified to deliver a working friction isolator mechanism that is able to prevent hunting cycles from occurring in a positioning system. The system behaved stable under the applied PID controller. Tuning the controller to the largest mass in the system yields a proper controller that is able to control all states of the system.

The placement of the cross-over frequency is mainly based on limitations in the surrounding system, through unavoidable internal resonances. For the best performance, it should be tuned as high as possible, such that settling times are as low as possible. A too low cross-over frequency is found to affect the working of the friction isolator, such that hunting cycles are still seen. In this case, the cross-over frequency should be placed in the range between 5.5 and 48 Hz.

In the experiments performed on the test setup, it was found that identifying the exact values for the friction forces is not realistic. However, it was also found that the exact values for the dynamic friction are not required for designing a compliant joint. It is sufficient to know whether stick-slip friction is present in a bearing and what the range of the static friction force is. From the parameter study, it was shown that there should at least be a gap between static and dynamic friction forces of around 1 N. It was further shown that the friction forces in the bearing can vary significantly without affecting the workings of the friction isolator.

After choosing a cross-over frequency, the compliant joint can be designed. It should be designed such that the drive stiffness of the system is as low as possible, while keeping the undamped parasitic frequencies around 10 times higher than the desired cross-over frequency. A lower drive stiffness induces a smaller required stroke of the compliant joint, which should be in the order of at least 0.3 mm.

5 Discussion

Parameter study

The system with the friction isolator shows some oscillatory behavior in certain simulations due to the internal mode, which leads to more peaks being identified than there are hunting cycles present in a simulation. It is however observed that hunting cycles are always present when peaks are identified. This means that the amount of peaks that are present is not a proper quantitative measure for the number of hunting cycles, but it is true that stable hunting cycles are present when peaks are identified. This conclusion also holds for the non-isolated system since parameters like the cross-over frequency influence the response time of the system, thus influencing the number of hunting cycles that can be present in an amount of time.

The parameter study is performed using 2d parameter grids, since there are too many parameters to fit in one grid. This decision does induce that not all relations between all parameters are taken into account. Though, the parameter grids are created such that the parameters that affect each other most are combined and thus the most important relations are evaluated. Combining the results of all the grids gives useful insights into the parameters that can be applied to all cases.

From the parameter study it is found that increasing the mass can be a way to prevent hunting from occurring in a system. However, this method has some drawbacks since a higher mass is often not preferred in servo systems. The system will become bulkier and larger actuators might be necessary. The conclusions of the parameter study should thus be evaluated for the specific system in order to verify whether it is really useful.

Control

In this research, a standard PID controller is applied to the positioning system. Other studies suggest that using other control methods positioning performance could be improved as well [7, 13, 15]. However, since a PID controller is well known and used widely in industry, this is deemed a suitable controller for this type of system. The motion controller used in the test setup was also not able to incorporate other control actions, confirming the standardized use of PID controllers. The use of different control strategies to prevent hunting is out of scope of this research.

Friction forces

The friction forces in the bearing are not exactly identified, due to limitations in the motion controller and position dependent variations in the friction forces. This has the consequence that the simulations do not exactly coincide with the experiments on the test setup. Though similar trends can be seen between the simulations and the experiments. Further, not being able to identify the friction forces in a bearing precisely, means that it is an unpredictable force. The friction isolator is shown to be a robust method to avoid problems due to this unpredictable force in the parameter study.

6 Conclusion

The performed parameter study on the main parameters of a friction isolator system showed that a limited bandwidth of the applied PID controller and a significant gap between static and dynamic friction forces are required in a positioning system for hunting cycles to occur. The path that is followed by the positioning system cannot be changed to robustly prevent hunting cycles from occurring.

Introducing a compliant joint in a system that suffers from hunting cycles, can prevent these unwanted cycles. It is found that the drive stiffness of this compliant joint should be as low as possible, for the best mitigation of hunting cycles. The design of the compliant joint is limited by the parasitic frequencies that are introduced by this mechanism and the stiffness in supporting directions. The parameter study showed that the friction isolator is a robust method to mitigate hunting cycles against various friction values.

The experimental setup that is built in this research showed mitigation of hunting cycles using a friction isolator for a control bandwidth of only 5 Hz, while the non-isolated system requires a higher bandwidth of 15 Hz. A compliant joint stroke of 0.3 mm is sufficient to prevent hunting from occurring. These experiments verify that the friction isolator is a suitable solution for systems that show hunting behavior.

7 Acknowledgements

The author would like to express his gratitude towards Heidenhain Nederland B.V. for generously lending the Etel AccurET position controller and the optical encoder and for their technical advice and support regarding these components. Equally deserving of gratitude is Technotion, for their provision of the linear actuator utilized in the test setup.

References

[1] Yoshihiro Maeda and Makoto Iwasaki. Rolling friction model-based analyses and compensation for slow settling response in precise positioning. *IEEE Transactions on Industrial Electronics*, 60(12), 2013.

[2] Farid Al-Bender and Jan Swevers. Characterization of Friction Force Dynamics. *IEEE Control Systems Magazine*, 28(6):64–81, 2008.

[3] Henrik Olsson. *Control Systems with Friction*. PhD thesis, Lund institute of technology, Lund, 1996.

[4] Ron H.A. Hensen and Marinus J.G. Van de Molengraft. Friction induced hunting limit cycles: An event mapping approach. *Proceedings of the American Control Conference*, 3:2267–2272, 2002.

[5] Ron H.A. Hensen, Marinus J.G. Van de Molengraft, and Maarten Steinbuch. Friction induced hunting limit cycles: A comparison between the LuGre and switch friction model. *Automatica*, 39(12):2131–2137, 12 2003.

[6] Xin Dong, Deokkyun Yoon, and Chinedum E. Okwudire. A novel approach for mitigating the effects of pre-rolling/pre-sliding friction on the settling time of rolling bearing nanopositioning stages using high frequency vibration. *Precision Engineering*, 47:375–388, 1 2017.

[7] Xin Dong, Xingjian Liu, Deokkyun Yoon, and Chinedum E. Okwudire. Simple and robust feedforward compensation of quadrant glitches using a compliant joint. *CIRP Annals - Manufacturing Technology*, 66(1), 2017.

[8] Xin Dong and Chinedum E. Okwudire. An experimental investigation of the effects of the compliant joint method on feedback compensation of pre-sliding/pre-rolling friction. *Precision Engineering*, 54:81–90, 10 2018.

[9] Xin Dong and Chinedum E. Okwudire. Influence of design parameters on the effectiveness of friction isolators in mitigating pre-motion friction in mechanical bearings. *Mechatronics*, 71:102444, 11 2020.

[10] Jiamin Wang, Xin Dong, Oumar R. Barry, and Chinedum Okwudire. Friction-induced instability and vibration in a precision motion stage with a friction isolator. *JVC/Journal of Vibration and Control*, 28(15-16):1879–1893, 8 2022.

[11] Zhijun Yang, Youdun Bai, Xin Chen, and Chaoran Chen. Single-drive rigid-flexible coupling precision motion platform and realization method and application thereof, 2018.

[12] Liyun Su, Ruirui Huang, Hao Peng, and Zhijun Yang. Optimal Design for Parameters of Structure and Controller for Rigid-Flexible Coupling Motion Stage. *Proceedings of 2020 IEEE 9th Data Driven Control and Learning Systems Conference, DDCLS 2020*, pages 1188–1192, 11 2020.

[13] Hao Peng, Han Sun, Zhijun Yang, Wenchao Xue, and Sen Chen. Comparison of several active disturbance rejection control methods for rigid-flexible coupling motion stage. In *Chinese Control Conference, CCC*, volume 2019-July, 2019.

[14] Hao Peng, Zhijun Yang, Wenchao Xue, Ruirui Huang, and Yi Huang. The Design and Control of a Rigid-Flexible Coupling Positioning Stage for Enhanced Settling Performance. *Journal of Dynamic Systems, Measurement and Control, Transactions of the ASME*, 143(11), 2021.

[15] Yutai Wei, Ruirui Huang, Hao Peng, and Zhijun Yang. On Switching Control Design for Rigid-Flexible Coupling Motion Stage. In *2020 39th Chinese Control Conference (CCC)*, pages 2708–2712, 2020.

[16] Brian Armstrong-Hélouvry, Pierre Dupont, and Carlos Canudas De Wit. A survey of models, analysis tools and compensation methods for the control of machines with friction. *Automatica*, 30(7):1083–1138, 7 1994.

[17] C. Canudas de Wit, P. Lischinsky, K. J. Åström, and H. Olsson. A New Model for Control of Systems with Friction. *IEEE Transactions on Automatic Control*, 40(3), 1995.

[18] Karl Johan Astrom and Carlos Canudas-De-Wit. Revisiting the LuGre Friction Model. *IEEE Control Systems*, 28(6), 2008.

[19] Y. F. Liu, J. Li, Z. M. Zhang, X. H. Hu, and W. J. Zhang. Experimental comparison of five friction models on the same test-bed of the micro stick-slip motion system. *Mechanical Sciences*, 6(1), 2015.

[20] Adriaan van Zelst. Mitigating Friction Induced Limit Cycles With A Friction Isolator, Master thesis, University of Twente, 2021.

[21] Lawrence F Shampine, Mark W Reichelt, and Siam J Sci Comput. THE MATLAB ODE SUITE *. *Society for Industrial and Applied Mathematics*, 18(1):1–22, 1997.

[22] Johannes van Dijk and Ronald G K M Aarts. Analytical one parameter method for PID motion controller settings. In *Proceedings of the IFAC Conference on Advances in PID Control*, WeC2.4, pages 1–6. University of Brescia, 3 2012.

[23] Herman M J R Soemers. *Design principles for precision mechanisms*. University of Twente, Netherlands, 2010.

A Appendices

A.1 Test setup identification

In Figure 29 the Bode plots of ten identification runs of the non-isolated plant can be seen. Some noise between 10 and 100 Hz can be seen in the magnitude plot. These identification runs are performed on different positions on the linear guide rail to get an averaged Bode plot.

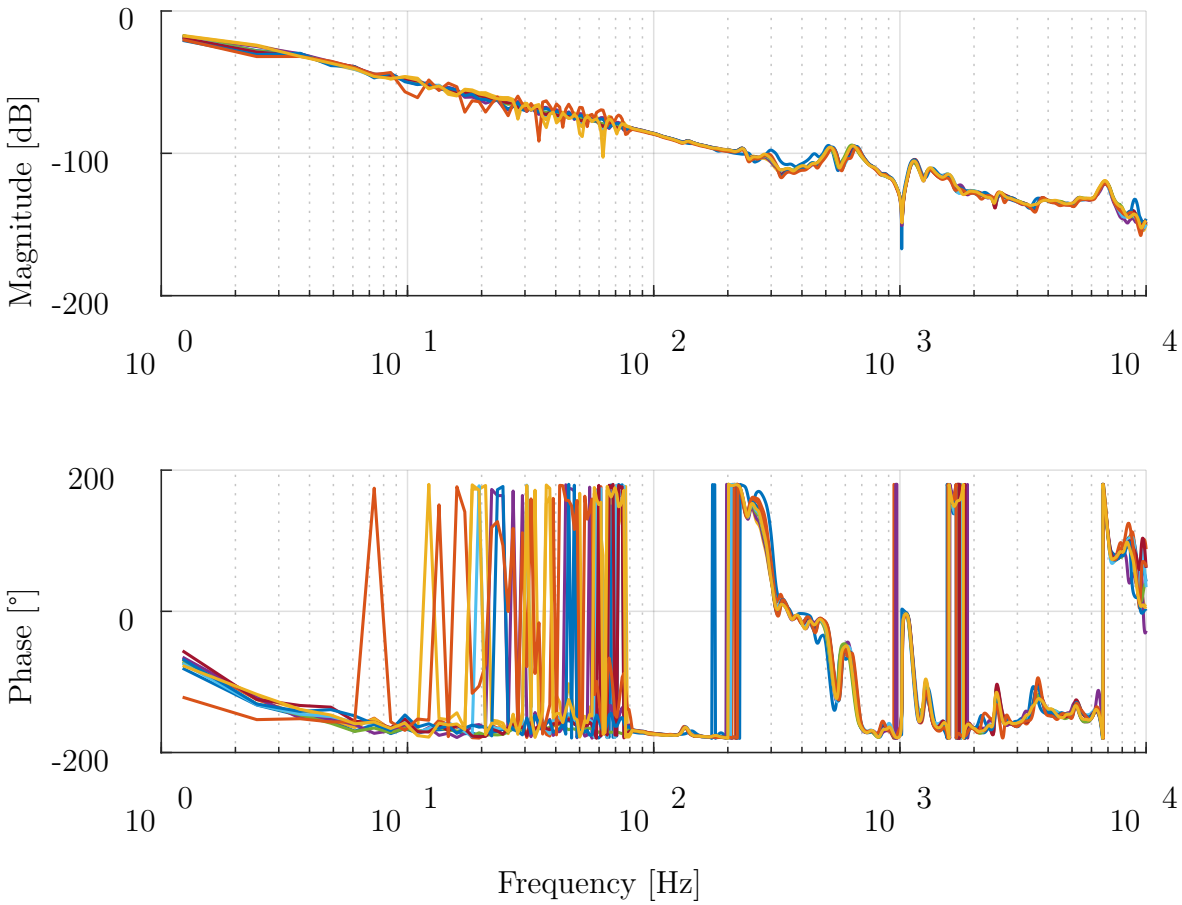

Figure 29: Bode plots of 10 identification runs of the non-isolated plant.